University of Alberta

Numerical simulation of Ricci flow on a class of manifolds with non-essential minimal surfaces

by

Jason Wilkes

A thesis submitted to the Faculty of Graduate Studies and Research
in partial fulfillment of the requirements for the degree of

Master of Science
in
Mathematical Physics

Department of Mathematical and Statistical Sciences

Fall 2011
Edmonton, Alberta

Examining Committee

Eric Woolgar, Mathematics and Statistical Sciences

Roger Moore, Physics

Youssef Belhamadia, Mathematics and Statistical Sciences

Henry van Roessel, Mathematics and Statistical Sciences

ABSTRACT

In the last three decades, the Ricci flow has proved to be an extremely useful tool in mathematics and physics, and its footprint is now visible on enterprises from the study of nonlinear sigma models in theoretical physics [7], to the proof of the geometrization conjecture for closed 3-manifolds and thus the Poincaré conjecture [15].

We explore numerically the long time existence of the Ricci-DeTurck flow and the List flow for a one-parameter family of Riemannian manifolds with non-essential minimal surfaces. This class of metrics is constructed to be an intermediate case between the corseted spheres examined by Garfinkle and Isenberg [8], and the $\mathbb{RP}^3$ geon explored by Balehowsky and Woolgar [2]. We find that the Ricci-DeTurck flow of these manifolds depends on the value of a geometric parameter k^2, with immortal flow below a critical value, and singularity formation above it. We also examine the List flow of this family of manifolds with and without a stable minimal surface, we compare the long-time existence properties to those observed in the case of the Ricci flow, and we use these results to gain insights into both the results obtained by Gulcev, Oliynyk, and Woolgar [10], and the general phenomena of singularity formation and critical behavior in Ricci flow.

ACKNOWLEDGEMENTS

First and foremost I would like to acknowledge my supervisor, Dr. Eric Woolgar. There is more than one sense in which I would not have completed this thesis without him. First, he was immediately willing and happy to help me switch from working with a previous supervisor to working with him. I am notoriously bad at working on things that do not interest me, and Dr. Woolgar helped me to find a research topic in which I was interested, and which gave me a long-desired excuse to learn some programming. Second, I cannot thank him enough for tolerating my endless questions and interruptions, whose obscenely high frequency was only possible as a result of his office being two steps away from mine. Thanks also to my mother, and to Michaela, my two favorite humans without a Y chromosome. They cannot help but make my life fun at every turn, and they have always supported the odd things I do. Finally, thanks to the University of Alberta for the financial support it has provided me over the past 2 years. It's an absolute scandal that one can be paid to go to school, and I owe the University much more than thanks for this.

To My Parents

Table of Contents

Chapter 1

Introduction to the Problem

> *But anyone who has experienced flow knows that the deep enjoyment it provides requires an equal degree of disciplined concentration.*
>
> −Mihály Csíkszentmihályi

Generally, a given differentiable manifold admits many Riemannian metrics. However, certain familiar manifolds, such as $\mathbb{R}^n$, S^n, and $\mathbb{H}^n$, admit what one might call a "canonical metric" – a metric that is in some sense "natural," and which exhibits a high degree of symmetry. Despite the intuitive appeal of this notion of a canonical metric, it is not clear *a priori* how to go about defining the concept rigorously, nor is it clear whether the notion can be given a rigorous definition in a sufficiently general context. We might think that we know what we mean when we speak of a canonical metric on $\mathbb{R}^n$, S^n, and $\mathbb{H}^n$; what do we mean by "canonical" for other Riemannian manifolds? Might it

be possible to formalize this idea?

In 1981, using the intuition that one should be able to evolve a manifold to such a canonical form, Richard Hamilton [11] invented the now famous Ricci flow. The Ricci flow is a set of nonlinear weakly parabolic partial differential equations, which attempts to diffuse the curvature of an initial metric[1] in much the same way that heat diffuses away from an initially concentrated heat source.

In the three decades since its inception, Ricci flow and its subsequent elaborations (e.g., [15], [5]) have provided mathematicians with a highly useful set of tools for studying the different geometries that a given manifold admits. The flow has found applications in theoretical physics, where it has been shown to arise from the renormalization group flow of a nonlinear sigma model [21], [7], and modifications of the Ricci flow (such as the Ricci-DeTurck flow and List's flow [12]) have proved useful in the study of general relativity [20]. The Ricci flow has even gained cursory fame among non-mathematicians, following its use in Perelman's proof of the geometrization conjecture for closed 3-manifolds [15], [16], [17], from which the famous Poincaré conjecture follows as a special

[1]Though as we will see, the curvature does not always diffuse away. The examples we examine, in which the flow halts due to the collapse of a "throat-like" portion of the manifold, provide an illustration of this fact. A simpler example is the (non-volume-normalized) flow of S^n, in which the flow, having "spread-out" the curvature as much as possible, collapses the manifold to a point in finite time.

case.

A general feature of the flow is that it tends to converge to metrics considered to be "canonical" in some sense. The flow thus provides, at least in part, a rigorous basis for the aforementioned intuitive notion. For example, if we start the flow from a two dimensional manifold with genus ≥ 2 it eventually (with proper rescaling) converges to a hyperbolic metric of constant negative curvature. However, certain initial metrics do not flow to a canonical metric in any sense of the word, but rather develop singularities after finite time. If we want to understand the Ricci flow, then it is important that we develop an understanding of these singularities, as well as the conditions under which they arise, and whether they can be meaningfully classified.

Garfinkle and Isenberg [8] began a research program of studying Ricci flow singularities numerically, and our purpose is to continue this exploration. We explore both the Ricci flow and the List flow of a class of manifolds described in chapter 3. The general form of the questions we consider is: Suppose we have a one parameter[2] family of manifolds, which will serve as our initial data. Is there some value of the parameter below which the Ricci flow converges to a "nice" (i.e. canonical) metric? Is there some value of the parameter above which the Ricci flow develops singularities in finite time? Is there some

[2]This parameter typically describes some feature of the initial geometry. In our case the parameter is the ratio of the areas of the "equator" S^2 and the "throat" S^2 of a slice of a Schwarzschild metric glued to a 3-sphere. See chapter 3 for details.

threshold value for which the flow exhibits qualitatively different behavior?

In their original paper on the topic [8], Garfinkle and Isenberg studied a one-parameter family of "corseted sphere" metrics on S^3, parametrized by the amount of curvature at the neck pinch. Using numerical methods, they found that metrics with a sufficiently small amount of corseting will flow to the canonical round metric on S^3, whereas metrics with a large amount of corseting become singular after finite time as the "throat" (S^2 minimal surface) collapses.

What's more, they found that for a certain value of the parameter, the geometry neither flows to the round metric on S^3 nor collapses, but instead exhibits qualitatively different behavior. For this value of the parameter, the flow was seen to converge on what they call a "javelin" geometry, with curvature singularities at both poles, but approximately uniform curvature in between. In a later paper, Garfinkle and Isenberg [9] found that this critical geometry exhibits so-called degenerate neck pinch singularities, which are well modeled by Bryant Solitons.

These results immediately suggest the question: Is this threshold behavior a quirk of the particular class of metrics Garfinkle and Isenberg examined, or might this behavior be a more universal feature of Ricci flow applied to one-parameter families? The class of manifolds I examine below will address this question.

In chapter 2, we define the Ricci flow, and discuss some basic results in the field, as well as extensions such as the Ricci-DeTurck flow and the List flow. In chapter 3, we define our initial data, for the flow by gluing together coordinate systems for S^3 and a slice of Schwarzschild spacetime. We also discuss our boundary conditions, and provide geometric motivation for them. In chapter 4, we discuss the numerical methods that we employ in our simulations, and rudiments of how they work. We then describe a numerical singularity, and discuss how to fix the problems arising from it, in the hope that this discussion might benefit others who wish to pursue numerical simulations of rotationally symmetric Ricci flow. Finally, in chapter 5, we summarize our results. First, we examine the rotationally symmetric Ricci-DeTurck flow with a minimal surface. We find that a critical parameter value separates the flow into two domains. For sufficiently large values, the manifold collapses, while for sub-critical values, the flow exists for all time. This is similar to the threshold behavior observed by Garfinkle and Isenberg [8], and our results therefore suggest that this behavior may be a common feature of the Ricci-DeTurck flow applied to one parameter families. Next, we examine the long-time existence of the List flow without an initial minimal surface. Here, we find that the rotationally symmetric, asymptotically flat List flow exists for all time, thus addressing a question raised recently by Gulcev, Oliynyk, and Woolgar [10]. Finally, we examine the List flow with an initial minimal surface. In this con-

text, as in the Ricci-DeTurck case, we find threshold behavior. However, there is no single critical value, but rather the point of transition from smooth flow to collapse depends on the parameters of the initial scalar field. In addition, we find that this field appears to increase the likelihood of collapse. That is, a geometry whose Ricci-DeTurck flow exists for all time may well collapse in the case of List flow with a minimal surface.

Chapter 2

The Basics of Ricci Flow

2.1 Defining the Flow

In what follows I will use index notation for tensors. To facilitate reading, I will use a, b, c, d to stand for uncontracted indices, and i, j, k, ℓ to stand for contracted indices. Let M be a Riemannian manifold of dimension n, and let $\{x^\ell\}_{\ell=1}^n$ be a system of coordinates for M. For a fixed metric g on M, we define the Christoffel Symbols by

$$\Gamma^a_{bc} = \frac{1}{2} g^{a\ell} \left(\frac{\partial g_{\ell b}}{\partial x^c} + \frac{\partial g_{\ell c}}{\partial x^b} - \frac{\partial g_{bc}}{\partial x^\ell} \right) \tag{2.1}$$

The Riemann Curvature Tensor can be defined in terms of the Christoffel symbols as follows:

$$R^a{}_{bcd} = \partial_c \Gamma^a_{bd} - \partial_d \Gamma^a_{bc} + \Gamma^a_{c\ell} \Gamma^\ell_{bd} - \Gamma^a_{d\ell} \Gamma^\ell_{bc} \tag{2.2}$$

We then define the Ricci Tensor in terms of the Riemann curvature tensor by:

$$R_{ab} := R^{\ell}{}_{a\ell b} = g^{\ell k} R_{a\ell bk} = g^{\ell k} R_{\ell akb} = \partial_\ell \Gamma^\ell_{ab} - \partial_b \Gamma^\ell_{a\ell} + \Gamma^\ell_{ab}\Gamma^k_{\ell k} - \Gamma^k_{a\ell}\Gamma^\ell_{bk} \quad (2.3)$$

Now, let $g(t)$ be a 1-parameter family of Riemannian Metrics on M, where $t \in [0, T) \subseteq \mathbb{R}$. The Ricci Flow consists of the following system of quasilinear partial differential equations

$$\frac{\partial}{\partial t} g_{ab} = -2R_{ab} \quad (2.4)$$

It was first proved by Hamilton [11], and later proved more simply by DeTurck [5] that if M is closed and $\tilde{g}$ is a C^∞ metric on M, then there exists some $\epsilon > 0$ such that the Ricci Flow has a unique solution $g(t)$ for $t \in [0, \epsilon)$ with initial data $\tilde{g}$ (i.e. $g(0) = \tilde{g}$). This is a short-time existence theorem for the Ricci flow. The question of long time existence is complicated by the development of singularities, and it is this question that we plan to examine.

2.2 The DeTurck Trick

Unfortunately for our purposes, the Ricci flow equation (2.4) is only weakly parabolic, and numerical analyses of weakly parabolic systems are often ill-posed. Moreover, even in well-posed cases, they are frequently unstable. Since we plan to examine the collapse of our manifold numerically (see chapter 4), we can use the so-called "DeTurck trick" to transform the weakly parabolic

Ricci flow (2.4) into the strongly parabolic Ricci-DeTurck flow [5]:

$$\frac{\partial}{\partial t} g_{ab} \overset{DeTurck}{=} -2R_{ab} + \pounds_X g_{ab} = -2R_{ab} + \nabla_a X_b + \nabla_b X_a \tag{2.5}$$

where the one form X_a is defined to be

$$X_a = g_{ak} g^{ij} \left(\Gamma^k_{ij} - \tilde{\Gamma}^k_{ij} \right) \tag{2.6}$$

Γ^a_{bc} are the Christoffel symbols arising from g_{ab} via (2.1), and $\tilde{\Gamma}^a_{bc}$ are the Christoffel symbols arising from a given fiducial metric. Notice that the non-tensorial Christoffel symbols appear in the definition of X_a. However, since the coordinate transformation law for Γ^k_{ij} is

$$\Gamma'^k_{ij} \frac{\partial x^\ell}{\partial x'^k} = \Gamma^\ell_{pq} \frac{\partial x^p}{\partial x'^i} \frac{\partial x^q}{\partial x'^j} + \frac{\partial^2 x^\ell}{\partial x'^i \partial x'^j} \tag{2.7}$$

the difference of two connections is

$$\left(\Gamma'^k_{ij} - \tilde{\Gamma}'^k_{ij} \right) \frac{\partial x^\ell}{\partial x'^k} = \left(\Gamma^\ell_{pq} - \tilde{\Gamma}^\ell_{pq} \right) \frac{\partial x^p}{\partial x'^i} \frac{\partial x^q}{\partial x'^j} + \left(\frac{\partial^2 x^\ell}{\partial x'^i \partial x'^j} - \frac{\partial^2 x^\ell}{\partial x'^i \partial x'^j} \right) \tag{2.8}$$

The two terms on the far right cancel, and so the difference between two Christoffel connections transforms as a tensor. This is why the definition of the DeTurck vector requires the fiducial connection $\tilde{\Gamma}^a_{bc}$. The equation (2.5) is strongly parabolic (see [3], pages 78-81). That is:

$$R_{ab} = -\frac{1}{2} \Delta g_{ab} - Q_{ab}(g^{-1}, \partial g) \tag{2.9}$$

so

$$\frac{\partial g_{ab}}{\partial t} = \Delta g_{ab} + Q_{ab}(g^{-1}, \partial g) \tag{2.10}$$

Thanks to the strong parabolicity provided by the DeTurck trick, the system is now more amenable to numerical methods than (2.4).

Moreover, if $g(t)$ is a solution to (2.5), then the pullback $\phi_t^* g(t)$ of $g(t)$ by a set of time-dependent diffeomorphisms ϕ_t generated by X is a solution to (2.4) for the same values of t (see [3] for a more extensive discussion of the DeTurck trick). Having solved (2.5), whether numerically or analytically, we indirectly obtain a solution to the Ricci flow (2.4) as follows. First notice that

$$\left.\frac{\partial}{\partial s}\right|_{s=0} \left(\phi_t^{-1} \circ \phi_{s+t}\right) = \left(\phi_t^{-1}\right)_* \left(\left.\frac{\partial}{\partial s}\right|_{s=0} \phi_{s+t}\right) = \left(\phi_t^{-1}\right)_* X(t) \tag{2.11}$$

Now, we can show that if $g(t)$ is a solution to the Ricci-DeTurck flow, then $\phi_t^* g(t)$ is a solution to the Ricci flow.

$$\begin{aligned}
\frac{\partial}{\partial t}\left(\phi_t^* g(t)\right) &= \left.\frac{\partial}{\partial s}\right|_{s=0} \left(\phi_{s+t}^* g(s+t)\right) \\
&= \phi_t^* \left(\frac{\partial}{\partial t} g(t)\right) + \left.\frac{\partial}{\partial s}\right|_{s=0} \left(\phi_{s+t}^* g(t)\right) \\
&= \phi_t^* \left(-2\mathrm{Ric}(g(t)) + \pounds_{X(t)} g(t)\right) \\
&+ \left.\frac{\partial}{\partial s}\right|_{s=0} \left(\left(\phi_t^{-1} \circ \phi_{s+t}\right)^* \phi_t^* g(t)\right) \\
&= -2\mathrm{Ric}\left(\phi_t^* g(t)\right) + \phi_t^* \left(\pounds_{X(t)} g(t)\right) - \pounds_{\left[\left(\phi_t^{-1}\right)_* X(t)\right]} \left(\phi_t^* g(t)\right) \\
&\overset{\text{By } (2.11)}{=} -2\mathrm{Ric}\left(\phi_t^* g(t)\right)
\end{aligned} \tag{2.12}$$

as desired. Therefore, given a solution $g(t)$ to the strongly parabolic Ricci-DeTurck flow, we obtain a solution $\phi_t^* g(t)$ to the weakly parabolic Ricci version. This fact can be exploited to stabilize the numerics in a numerical simulation of

(2.4). Thanks to this result, even though we numerically implement the Ricci-DeTurck flow, which is much easier to deal with, we can obtain a solution to the Ricci flow if desired.

2.3 Building Intuition About the Ricci Flow

In the introduction, we mentioned that the Ricci flow attempts to diffuse the curvature of an initial metric in much the same way that heat diffuses away from an initially concentrated heat source. Anyone who has seen a visual simulation of Ricci flow[1] will have an intuitive understanding of this idea. Is there any way in which we might make this intuition more precise? After all, the heat equation with source

$$\frac{\partial u}{\partial t} = \Delta u + Q \tag{2.13}$$

where $u = u(t, x_1, ..., x_n)$ represents the temperature of a body, and $Q = Q(t, x_1, ..., x_n)$ is a known function that represents the body's internally generated heat per unit volume[2], is known to simulate well the diffusion of sub-

[1]See `http://www.irp.oist.jp/mbu/sinclair/ricci_rot/ricci_rot.mov` for a visual simulation of Ricci flow by J. Hyam Rubinstein and Robert Sinclair. The visualization method is described in [19].

[2]This quantity is often set to zero, as most objects internally generate a negligible amount of heat. However, if one wanted to examine, say, the steel coils on a conventional stove, then the function Q above would be a non-negative function with support on the coils when the stove is turned on, and zero when the stove is turned off.

stances other than heat. However, the Ricci flow equation does not, at first glance, appear very similar to this equation, at least in the form (2.4) above.

Despite the superficial difference, there are some similarities. The heat equation is the most natural example of a parabolic partial differential equation, and as we mentioned above, the Ricci flow equation is either strongly or weakly parabolic, depending on whether or not one employs the DeTurck trick. Moreover, both the Ricci flow equation and the heat equation contain first order time derivatives of their dynamical variables g and u respectively, as well as second order spatial derivatives. Equation (2.10) makes the analogy with the heat equation precise. When written in the form of (2.10), we can see that the Ricci flow can be understood as a heat equation for the metric components g_{ij}, with heat source $Q_{ij}(g^{-1}, \partial g)$.

2.4 A Heat Equation for the Ricci Scalar

The quantity that "diffuses" under the heat equation is the temperature u, and the analogy with the heat equation together with (2.10) suggests that we should view the *metric* as the object that diffuses under Ricci flow. Thus, we have still not codified the intuition that it is the *curvature*, in some sense, that diffuses under Ricci flow. However, from (2.4) one can also derive the evolution equations for the tensors $R^a{}_{bcd}$, R_{ab} and R. The following proposition finally makes rigorous the intuition that the Ricci flow represents a diffusion

of *curvature* in particular.

Proposition 2.1. *If g_{ab} is a solution to the Ricci flow equation, then*

$$\frac{\partial R}{\partial t} = \Delta R + 2R^{ij}R_{ij} \tag{2.14}$$

Note, the quantity $R^{ij}R_{ij}$ is often written $|\mathrm{Ric}|^2$

Proof. Let g_{ab} be a solution to the Ricci flow equation, and let R^a_{bcd},R_{ab},and R be the Riemann, Ricci, and scalar curvatures associated with g_{ab}. Then

$$0 = \partial_t(\delta^a_b) = \partial_t(g^{a\ell}g_{\ell b}) = g_{cb}\partial_t g^{ac} - 2g^{ac}R_{cb} \tag{2.15}$$

So $\partial_t g^{ij} = 2R^{ij}$. Also recall $\nabla\left(R^{ab} - \frac{1}{2}Rg^{ab}\right) = 0$. Now:

$$\frac{\partial R}{\partial t} = \frac{\partial}{\partial t}\left(g^{ij}R_{ij}\right) = \left(\frac{\partial}{\partial t}g^{ij}\right)R_{ij} + g^{ij}\left(\frac{\partial}{\partial t}R^{ij}\right) \tag{2.16}$$

$$= 2R^{ij}R_{ij} + g^{ij}\left[\Delta_L R_{ij} - \nabla_i\nabla^k R_{jk} - \nabla_j\nabla^k R_{ik} + \nabla_i\nabla_j R\right]$$

$$= 2R^{ij}R_{ij} + g^{ij}\left[\Delta R_{ij} - R_i{}^k R_{jk} - R_j{}^k R_{ik} + R^{k\ l}_{i\ j}R_{kl} + R^{k\ l}_{j\ i}R_{kl}\right]$$

$$- g^{ij}\left[\nabla_i\nabla^k R_{jk} - \nabla_j\nabla^k R_{ik} + \nabla_i\nabla_j R\right]$$

$$= 2R^{ij}R_{ij} + \left[\Delta R - R^{jk}R_{jk} - R^{ik}R_{ik} + g^{ij}R^{kl}\left(R_{kilj} + R_{kjli}\right)\right]$$

$$- \left[\nabla_j\nabla_k R^{jk} - \nabla_i\nabla_k R^{ik} + \Delta R\right]$$

$$= 2R^{ij}R_{ij} + \left[2\Delta R - 2R^{ij}R_{ij} + 2g^{ij}R^{kl}R_{kilj} - 2\nabla_i\nabla_j R^{ij}\right]$$

$$= 2\left(\Delta R + 2g^{ij}R^{kl}R_{ikjl} - \nabla_i\left(\frac{1}{2}g^{ij}\nabla_j R\right)\right)$$

$$= 2\left(\Delta R + R^{kl}R_{kl} - \frac{1}{2}g^{ij}\nabla_i\nabla_j R\right) = 2\left(\Delta R + R^{kl}R_{kl} - \frac{1}{2}\Delta R\right)$$

$$\boxed{\frac{\partial R}{\partial t} = \Delta R + 2R^{ij}R_{ij}} \tag{2.17}$$

□

as desired. Note that this is exactly the scalar heat equation (2.13) with "temperature" $u = R$, and internally generated "heat" (scalar curvature) per unit volume $Q = 2R^{ij}R_{ij} = 2\left|\mathrm{Ric}\right|^2$.

For the Ricci-DeTurck flow (2.5), carrying out a slightly modified version of this argument gives

$$\frac{\partial R}{\partial t} \;=\; \Delta R + 2R^{ij}R_{ij} + X^i\nabla_i R \;=\; \left(\frac{\partial R}{\partial t}\right)_{Ricci} + \pounds_X R \tag{2.18}$$

2.5 Some Exact Solutions of the Ricci Flow Equation

The Ricci flow is a highly nonlinear set of coupled partial differential equations. It is no surprise, therefore, that we cannot solve this equation analytically in most circumstances. Even so, in the same way that physicists build intuition through the construction of "toy models" − models not meant to be physically realistic, but which in their simplicity manage to illustrate the basic principles encountered in more complex cases − we can gain considerable intuition about the Ricci flow by examining somewhat trivial but nevertheless important cases in which the equations can be solved exactly. One such case is the family of

Einstein metrics.

Let $g(0) = \tilde{g}$ be an Einstein metric. That is, assume

$$\mathrm{Ric}(\tilde{g}) = \alpha\tilde{g} \tag{2.19}$$

where $\alpha \in \mathbb{R}$. We will build solutions to the Ricci Flow equation (2.4) by letting $g(t) = \gamma(t) \cdot \tilde{g}$ and placing constraints on the positive-valued function $\gamma(t)$. Notice that by definition of the Ricci tensor in terms of the Christoffel symbols, we have $\mathrm{Ric}(g(t)) = \mathrm{Ric}(\gamma(t)\tilde{g}) = \mathrm{Ric}(\tilde{g}) = \alpha\tilde{g}$. By (2.4) we have

$$\frac{\partial}{\partial t}g(t) = \frac{\partial}{\partial t}\left[\gamma(t)\tilde{g}\right] = \gamma'(t)\tilde{g} = -2\mathrm{Ric}(g(t)) = -2\alpha\tilde{g} \tag{2.20}$$

So $\gamma'(t) = -2\alpha$, and thus we have $\gamma(t) = -2\alpha t + \gamma(0) = -2\alpha t + 1$ Therefore, we have found an exact solution to the Ricci Flow

$$g(t) = (1 - 2\alpha t)\tilde{g} \tag{2.21}$$

We call the $\alpha < 0$, $\alpha = 0$, and $\alpha > 0$ cases *expanding*, *steady*, and *shrinking* respectively. This terminology is motivated by the following calculation: Recall that the volume of a Riemannian Manifold (M, g) is

$$Vol(M, g) = \int_M \sqrt{det(g)}d^n x \tag{2.22}$$

provided the integral is defined. Plugging our solution to the Ricci Flow equation into this formula gives

$$Vol(M, g(t)) = \int_M \sqrt{det(g(t))}d^n x = (1 - 2\alpha t)^{\frac{n}{2}} \int_M \sqrt{det(\tilde{g})}d^n x \tag{2.23}$$

And thus

$$Vol(M, g(t)) = (1 - 2\alpha t)^{\frac{n}{2}} Vol(M, \tilde{g}) \tag{2.24}$$

This helps us make sense of the above terminology. If $\alpha < 0$, then $Vol(M, g(t))$ is an increasing function of time, so we say $g(t)$ is *expanding*. Similarly, if $\alpha > 0$, then $Vol(M, g(t))$ is decreasing, so we say $g(t)$ is *shrinking*. Finally, if $\alpha = 0$, then $Vol(M, g(t)) = Vol(M, \tilde{g})$ is constant, and we say $g(t)$ is *steady*. Notice that if $g(t)$ is *shrinking*, then $g\left(\frac{1}{2\alpha}\right) = 0$, so the solution only exists for $t \in \left[0, \frac{1}{2\alpha}\right)$.

The canonical metrics on S^n, $\mathbb{R}^n$, and $\mathbb{H}^n$ are all Einstein [13], and thus their flows can can be solved exactly, as above. The Ricci flow of S^n collapses the manifold to a point in finite time (at which point the flow stops), whereas the flows of $\mathbb{R}^n$ and $\mathbb{H}^n$ exist for all $t \geq 0$.

Another class of metrics for which the flow simplifies considerably is the class of Ricci solitons [20], [21]. A Ricci soliton is a metric that satisfies:

$$\frac{\partial g_{ab}}{\partial t} = c g_{ab} \tag{2.25}$$

That is, the manifold remains self-similar under the flow. Plugging this definition into the Ricci-DeTurck equation gives us the so-called Ricci soliton equation:

$$R_{ab} - \frac{1}{2}\pounds_X g_{ab} - c g_{ab} = 0 \tag{2.26}$$

where I have absorbed a constant into c. Due to a result dicussed in a recent preprint by Figueras, Lucietti, and Wiseman [6], an appropriate choice of

boundary conditions prevents the flow from converging to a soliton. As we will discuss later in section 3.5, one of our boundary conditions at "pseudo-infinity," namely setting the DeTurck vector $X = 0$, is just such a boundary condition.

Now, since we can solve the flow equations exactly both for spheres S^n, and for Euclidean spaces $\mathbb{R}^m$, we can solve the flow equations exactly for "cylinders" $S^n \times \mathbb{R}^m$. A special case of this, namely segments of $S^2 \times \mathbb{R}$, provide a kind of toy model for the study of certain types of singularity formation, including "collapse at a neck" − the type of singularity we will be most concerned with. For a Riemannian metric g on a manifold M, we say M contains an ϵ-neck centered at a point $x \in M$ if there exists a diffeomorphism

$$F : S^2 \times (-\epsilon^{-1}, \epsilon^{-1}) \longrightarrow M \tag{2.27}$$

where $F^{-1}(x) \in S^2 \times 0$, and such that the metric $R(x)F^*g$ (where $R(x)$ is the scalar curvature at $x \in M$) is within ϵ of the canonical metric $g_{S^2(\sqrt{2})} \times \delta$ on $S^2(r = \sqrt{2}) \times (-\epsilon^{-1}, \epsilon^{-1})$ with respect to a certain topology[3]. The scale r_M of an ϵ-neck in M centered at x is defined to be $R(x)^{-1/2}$. This gives a measure of the radius of the smallest S^2 in the neck, and thus in the context of Ricci flow, it gives us a rough measure of how close a given segment of a manifold is to collapse. Now let $\tilde{g}$ be the round metric on $S^2(\sqrt{2})$, and consider the Ricci flow with initial metric $\tilde{g}$. Then $g(t) = (1-t)\tilde{g}$ is an exact solution to the Ricci flow

[3]The so called $C^{[1/\epsilon]}$-topology. For a definition of this topology, see [13].

equation for $t \in (-\infty, 1)$. We may also consider a trivial generalization of this flow to $(S^2(\sqrt{2}) \times \mathbb{R}, h(t) \times \delta_{ij})$. This is called the standard shrinking round cylinder (see [13]), and it provides a model for the flow of ϵ-necks. This model is important in the study of Ricci flow singularities because such singularities often develop as a thin piece of the manifold, diffeomorphic to the product of S^2 and an interval, collapses under the flow. For example, in Garfinkle and Isenberg's numerical exploration of corseted S^3s [8], [9], they found that the critical value of the corseting parameter led the geometry to become "locally cylindrical in a neighborhood of the initial pinching". A cylinder is essentially an ϵ-neck. This is important because the Ricci flow that Garfinkle and Isenberg examined could not be solved exactly, but the flow of an ϵ-neck can be. So, for geometries that exhibit similar collapse behavior, and especially for the critical geometry in Garfinkle and Isenberg's case, considerable insight can be gained by studying an exactly solvable situation that approximates the case of interest. Though the analogy may not be obvious, this is exactly what we are doing in examining a numerical simulation: in such a simulation, we are *not* solving the Ricci flow equations − rather, we are inverting an exactly solvable matrix equation that behaves, in all the relevant ways, like the intractable Ricci flow. Both examples are instances of the same principle. This section examined exact solutions of the Ricci flow equation because doing so gives us insight into cases that cannot be solved exactly; the same principle is at work

in our choice to pursue a numerical approach in chapters 4 and 5.

We begin the discussion of our problem in chapter 3, and as we will see in chapter 5, there exist certain parameter values for which our manifold develops a singularity of the aforementioned type: collapse at a "neck."

2.6 The List Flow

The List flow was invented by Bernhard List in his dissertation under the direction of Gerhard Huisken [12]. The flow is constructed to converge on solutions of the static vacuum Einstein equations, and as such, its fixed points are of special interest. The defining equations arise from modifying the Ricci flow through the addition of a scalar field u, such that if (u, g) solves the List flow, then a certain combination of u and g gives a "spacetime" that solves the Ricci-DeTurck flow [21]. As a result, this flow has proved useful in the mathematical study of General Relativity. The List flow is defined by the equations:

$$\begin{aligned} \frac{\partial g_{ij}}{\partial t} &= -2\left(R_{ij} - \nabla_i u \nabla_j u\right) \\ \frac{\partial u}{\partial t} &= \Delta u \end{aligned} \tag{2.28}$$

If the pair (u, g) satisfies the above equations, then we can construct a "spacetime" metric from the pair (see [21], [12]) via

$$g_{\mu\nu}dx^\mu dx^\nu = \pm e^{2u}dt^2 + g_{ij}dx^i dx^j \tag{2.29}$$

such that the spacetime metric solves the Ricci-DeTurck flow with DeTurck vector $-\nabla u$. That is,

$$\frac{\partial g_{\mu\nu}}{\partial t} = -2R_{\mu\nu} + \pounds_{-\nabla u} g_{\mu\nu} \tag{2.30}$$

We are free to choose the sign of the temporal term in (2.29), and interesting but distinct results follow in each case. Choosing "$-$" gives us a Lorentzian signature, and since the fixed points of (2.28) satisfy $R_{ij} = \nabla_i u \nabla_j u$, the flow converges to a metric that obeys[4] the Einstein equation for a massless scalar field [21], [1]. Choosing "+" gives a Euclidean signature, and (with the addition of a cosmological term Λg_{ij}) the fixed points of the List flow will be Ricci solitons (see [1] for details). In the next section, we construct our initial data. We examine the List flow of this initial data in section 5.2.

[4]Of course, the fixed points of the List flow obey this condition whether we choose "+" or "$-$", but only in the "$-$" case does the Einstein equation have its usual (Lorentzian) form, and thus its usual (physical) interpretation.

Chapter 3

The Rotationally Symmetric Flow

3.1 Constructing the Initial Data

Recall that Garfinkle and Isenberg [8] found a 1-parameter family of corseted spheres for which the flow either terminated due to a neck pinch, or converged to a 3-sphere, depending on the value of the parameter. Moreover, they found critical behavior at the point that separates the two domains.

Balehowsky and Woolgar [2] explored a similar problem for their own 1-parameter family − a class of complete, noncompact manifolds with an essential minimal hypersphere. Their manifold is known as the $\mathbb{RP}^3$ Geon, and it arises as a quotient of a spacelike hypersurface of Schwarzschild spacetime.

While Garfinkle and Isenberg found threshold behavior, Balehowsky and Woolgar found collapse for all parameter values.

The Garfinkle and Isenberg result raises the question: Is this threshold behavior (collapse on one side, smooth flow on the other) a quirk of the particular class of metrics they examined, or might this behavior be a more universal feature of Ricci flow applied to one-parameter families? The manifold constructed here is designed to address this question. The initial data from which we will begin the flow is an intermediate case between Garfinkle and Isenberg's corseted 3-spheres, and the geometry examined by Balehowsky and Woolgar. The manifold below contains "corseting" in a sense, but this results from gluing a round (uncorseted) 3-sphere to the Schwarzschild slice in such a way that the minimal surface of the Schwarzschild slice becomes the minimal surface of our manifold.

In this section, we construct our initial data by gluing together a 3-sphere and the Schwarzschild slice. We proceed as follows:

3.2 The Round 3-sphere Portion

The standard metric on a round 3-sphere is

$$ds^2 = dR^2 + \sin^2(R)d\Omega^2 \tag{3.1}$$

For our purposes, it will be convenient to work with coordinates of the form:

$$ds^2 = e^{2A(r,t)}dr^2 + e^{2B(r,t)}r^2 d\Omega^2 \tag{3.2}$$

on both the 3-sphere portion and the Schwarzschild portion. Since our initial geometry will be both piecewise-smooth and time dependent, the general forms of $A(r,t)$ and $B(r,t)$ are intractably difficult to write down, which is why we work numerically. For now, though, we simply want to write down the form of these functions at time $t = 0$ on a particular piece of the geometry: the 3-sphere. For the initial metric from which we start the flow, we have $A(r,0) = B(r,0) := A(r)$ in the round 3-sphere portion. By setting the above two metrics equal to each other and solving for R in terms of r, we can obtain $A(r)$ in this part of the manifold. Equating (3.1) and (3.2) gives:

$$dR = e^{A(r)}dr \qquad\qquad \sin(R) = re^{A(r)} \tag{3.3}$$

These two equations together imply

$$\frac{dR}{dr} = \frac{\sin(R)}{r} \Longrightarrow \ln(r) = -\ln\left(\csc(R) + \cot(R)\right) + const \tag{3.4}$$

$$= \ln\left(k \cdot \frac{1+\cos(R)}{\sin(R)}\right) \Longrightarrow r = k \cdot \frac{1+\cos(R)}{\sin(R)} = k \cdot \frac{1+\cos(R)}{\sqrt{1-\cos^2(R)}}$$

$$r = k \cdot \frac{1+\cos(R)}{\sqrt{(1-\cos(R))(1+\cos(R))}} = k \cdot \sqrt{\frac{1+\cos(R)}{1-\cos(R)}}$$

Then

$$\cos(R) = \frac{(r/k)^2 - 1}{(r/k)^2 + 1} \Longrightarrow \sin(R) = \frac{\pm 2(r/k)}{1 + (r/k)^2} \tag{3.5}$$

and now by (3.3) we have $e^{A(r)} = \frac{(2/k)}{1+(r/k)^2}$, so squaring this and relabeling $\rho = \frac{r}{k}$ we can write the initial metric for the sphere portion as

$$ds^2 = \frac{4k^2}{\left(1+\rho^2\right)^2}\left(d\rho^2 + \rho^2 d\Omega^2\right) \tag{3.6}$$

where $\rho \in (0, \infty)$ and $d\Omega^2 = d\theta^2 + \sin^2(\theta)\, d\phi^2$. This coordinate system covers the 3-sphere everywhere except the north and south poles, corresponding to the values $\rho = \infty$ and $\rho = 0$ respectively. For $\rho \in (0, \infty)$ a surface of constant ρ is a 2-sphere of area

$$S(\rho) = \left(\frac{4k^2}{\left(1+\rho^2\right)^2}\right)\left(4\pi\rho^2\right) = \frac{16\pi^2 k^2}{\left(1+\rho^2\right)^2} \tag{3.7}$$

with mean curvature of

$$H(\rho) = \frac{1-\rho^2}{k\rho} \tag{3.8}$$

Notice that the combination

$$H^2(\rho)\, S(\rho) = 16\pi\left(\frac{1-\rho^2}{1+\rho^2}\right) \tag{3.9}$$

is independent of k. We will use this in the gluing phase. Since the equator of the 3 sphere corresponds to the zero locus of $H(\rho)$, we have

$$H(\rho) = 0 \Longrightarrow \rho = 1 \Longrightarrow S(\rho) = S(1) = 4\pi k^2 \tag{3.10}$$

3.3 The Schwarzschild Portion

As mentioned above, Balehowsky and Woolgar [2] examined the Ricci-DeTurck flow of the so-called $\mathbb{RP}^3$ Geon. This metric arises from the $t = 0$ slice of

the $(n+1)-$dimensional Schwarzschild-Tangherlini metric. The metric on a constant time hypersurface of Schwarzschild spacetime can be written in isotropic coordinates as

$$ds^2 = \left(\frac{1}{2r_0}\right)^2 \left(1+\frac{r_0}{2r}\right)^4 \left(dr^2 + r^2 d\Omega^2\right) \tag{3.11}$$

where $r \in (-\infty, \infty)$ and $d\Omega^2$ is as defined above. This coordinate system covers the constant time hypersurface of extended Schwarzschild spacetime everywhere. A surface of constant r gives a 2-sphere of area

$$S(r) = \left(\frac{4\pi r^2}{4r_0^2}\right)\left(1+\frac{r_0}{2r}\right)^4 \tag{3.12}$$

and mean curvature

$$H(r) = \left(\frac{4r_0}{r}\right)\left(\frac{1-\frac{r_0}{2r}}{\left(1+\frac{r_0}{2r}\right)^3}\right) \tag{3.13}$$

Notice that as in the 3-sphere case, the combination

$$H^2(r)\,S(r) = 16\pi\left(\frac{1-\frac{r_0}{2r}}{1+\frac{r_0}{2r}}\right)^2 = 16\pi\left(\frac{2r-r_0}{2r+r_0}\right)^2 \tag{3.14}$$

is independent of k. Since the throat (Event Horizon) of our Schwarzschild slice corresponds to the zero locus of $H(r)$, we have

$$H(r) = 0 \Longrightarrow r = \frac{r_0}{2} \Longrightarrow S(r) = S\left(\frac{r_0}{2}\right) = 4\pi \tag{3.15}$$

3.4 The Gluing Process

In this section, we join the two metrics as smoothly as possible. This gluing cannot be accomplished to all orders, but we will see that the first two orders

(joining the area S and the mean curvature H) is good enough. The ratio of the area of the 3-sphere's equator to the area of the throat of the Schwarzschild slice is k^2. That is,

$$\frac{S\left(\rho=1\right)}{S\left(r=\frac{r_0}{2}\right)}=\frac{S\left(H^{-1}\left(0\right)\right)}{S\left(H^{-1}\left(0\right)\right)}=\frac{4\pi k^2}{4\pi}=k^2 \tag{3.16}$$

First, notice that we can join these metrics only if $k^2 \geq 1$, and we get a stable minimal surface iff $k^2 > 1$. We will force the requirement $k^2 \geq 1$ in what follows.

We want to join these two metrics at some 3-sphere coordinate $\rho = \rho_J$ and some Schwarzschild coordinate $r = r_J$ (The subscript J is meant to be mnemonic for 'join'). We will accomplish this by forcing the areas and mean curvatures to match at these coordinate values. That is, we require the areas to match

$$\frac{16\pi^2 k^2}{\left(1+\rho_J^2\right)^2} \equiv S(\rho_J) = S(r_J) \equiv \left(\frac{4\pi r_J^2}{4r_0^2}\right)\left(1+\frac{r_0}{2r_J}\right)^4 \tag{3.17}$$

And the mean curvatures to match

$$\frac{1-\rho_J^2}{k\rho_J} \equiv H(\rho_J) = H(r_J) \equiv \left(\frac{4r_0}{r_J}\right)\frac{1-\frac{r_0}{2r_J}}{\left(1+\frac{r_0}{2r_J}\right)^3} \tag{3.18}$$

This occurs at some value $\rho_J \geq 1$, and $r_J \leq \frac{r_0}{2}$ If we square (3.18) and multiply the result by (3.17), we eliminate k. This is why we looked at $H^2\left(r\right)S\left(r\right)$ and $H^2\left(\rho\right)S\left(\rho\right)$ in (3.9) and (3.14) above. This gives us

$$\left(\frac{1-\rho_J^2}{1+\rho_J^2}\right)^2 = \left(\frac{1-\frac{r_0}{2r_J}}{1+\frac{r_0}{2r_J}}\right)^2 \tag{3.19}$$

So

$$\left(1-\rho_J^2\right)\left(2r_J+r_0\right)=\left(1+\rho_J^2\right)\left(2r_J-r_0\right) \tag{3.20}$$

And thus

$$r_0-2r_J\rho_J^2=-r_0+2r_J\rho_J^2 \quad\Longrightarrow\quad \rho_J=\sqrt{\frac{r_0}{2r_J}} \tag{3.21}$$

We have now "glued" the two metrics together, but we still have two coordinate systems as a vestige of the gluing process. To get a single coordinate system, we define a new coordinate 'r' in the sphere metric by $r\equiv\frac{r_J}{\rho_J}\rho$. Then $\rho=\rho_J\Longrightarrow r=r_J$, and so when $(r\leq r_J)$ the metric becomes

$$\begin{aligned} ds^2&=\left(\frac{2k\left(\rho_J/r_J\right)}{1+\left(\rho_J^2/r_J^2\right)r^2}\right)^2\left(dr^2+r^2d\Omega^2\right) \\ &=\left(\frac{2k\rho_Jr_J}{r_J^2+\rho_J^2r^2}\right)^2\left(dr^2+r^2d\Omega^2\right) \end{aligned} \tag{3.22}$$

Also, by (3.18) we have

$$k=\left(\frac{r_J\left(1-\rho_J^2\right)}{4r_0\rho_J}\right)\frac{\left(1+\frac{r_0}{2r_J}\right)^3}{1-\frac{r_0}{2r_J}}=\left(\frac{r_J}{4r_0\rho_J}\right)\left(1+\frac{r_0}{2r_J}\right)^3 \tag{3.23}$$

And now, using (3.21) we obtain

$$k=\left(\frac{r_J}{2r_0}\right)^{3/2}\left(1+\frac{r_0}{2r_J}\right)^3 \tag{3.24}$$

We can now express the sphere metric solely in terms of the global coordinate r, r_0, the join value r_J, and the metric $d\Omega^2$ on the 2-spheres:

$$ds^2=\frac{\left(1+\frac{r_0}{2r_J}\right)^6}{4r_0^2\left(1+\frac{r_0r^2}{2r_J^3}\right)^2}\left(dr^2+r^2d\Omega^2\right)\qquad\qquad(r\leq r_J) \tag{3.25}$$

Recall that r_0 originally appeared as a parameter in the Schwarzschild metric. Notice that $S_{throat} = S\left(\frac{r_0}{2}\right)$ is independent of r_0, so we are free to vary r_0 without changing the problem. We can simplify some of the above equations by choosing $r_0 = 2$. This gives

$$k^2 = \left[\left(\frac{r_J}{2r_0}\right)^{\frac{3}{2}}\left(1+\frac{r_0}{2r_J}\right)^3\right]^2 = \frac{r_J^3}{64}\left(1+\frac{1}{r_J}\right)^6 = \frac{1}{64}\left(\sqrt{r_J}+\frac{1}{\sqrt{r_J}}\right)^6 \quad (3.26)$$

In the spirit of item (3.16), we call k^2 the Area Ratio. The name is appropriate since k^2 is a geometric quantity not dependent on our particular choice of coordinates. Our choice to set $r_0 = 2$ also allows us to simplify the metric significantly. The metric is now

$$ds^2 = \begin{cases} \frac{1}{16}\left(1+\frac{1}{r}\right)^4\left(dr^2+r^2d\Omega^2\right) & : r \in [r_J, \infty) \\ \\ \frac{1}{16}\frac{\left(1+r_J^{-1}\right)^6}{\left(1+(r^2/r_J^3)\right)^2}\left(dr^2+r^2d\Omega^2\right) & : r \in (0, r_J] \end{cases}$$

The condition $r_J \leq \frac{r_0}{2}$ above now gives $r_J \leq 1$. Notice that

$$S(r) \equiv S(t=0,r) = \begin{cases} \frac{\pi r^2}{4}\left(1+\frac{1}{r}\right)^4 & : r \in [r_J, \infty) \\ \\ \frac{\pi r^2}{4}\frac{\left(1+r_J^{-1}\right)^6}{\left(1+(r^2/r_J^3)\right)^2} & : r \in (0, r_J] \end{cases}$$

Finally, we write the initial metric as

$$ds^2 = e^{2A(r)}dr^2 + \frac{S(r)}{4\pi}d\Omega^2 \quad (3.27)$$

or equivalently

$$ds^2 = e^{2A(r)}\left(dr^2+r^2d\Omega^2\right) \quad (3.28)$$

where the function $A(r)$ is defined to be

$$A(r) = \begin{cases} \log\left[\frac{1}{4}\left(1+\frac{1}{r}\right)^2\right] & : r \in [r_J, \infty) \\ \\ \log\left[\frac{1}{4}\frac{\left(1+r_J^{-1}\right)^3}{\left(1+(r^2/r_J^3)\right)}\right] & : r \in (0, r_J] \end{cases}$$

To summarize, this data defines a manifold that we constructed by gluing S^3 to Sch^3 (Sch^3 is shorthand for the Schwarzschild slice described in section 3.3). While we could use the shorthand $S^3 \# Sch^3$ to denote this space, even this is quite ugly, so we will simply refer to it as "the bubble." Figure 3.1 shows a simple representation of the bubble. As a last step, we can solve for the coordinate-dependent quantity r_J in terms of the geometrically meaningful Area Ratio k^2.

$$2k^{\frac{1}{3}} = \sqrt{r_J} + \frac{1}{\sqrt{r_J}} \quad \Longrightarrow \quad r_J - 2k^{\frac{1}{3}}\sqrt{r_J} + 1 = 0 \quad \Longrightarrow$$

$$\sqrt{r_J} = k^{\frac{1}{3}} \pm \sqrt{k^{\frac{2}{3}} - 1} \qquad \text{(Choose "}-\text{" since } k \geq 1 \text{ but } r_J \leq 1)$$

$$\Longrightarrow \quad r_J = 2\left(k^2\right)^{\frac{1}{3}} - 1 - 2\left(k^2\right)^{\frac{1}{6}}\sqrt{(k^2)^{\frac{1}{3}} - 1} \tag{3.29}$$

Looking at the initial data defined above, the reader might have noticed that

$$A(r) = \frac{1}{2}\log\left(\frac{S(r)}{4\pi r^2}\right) \tag{3.30}$$

so

$$e^{2A(r)} = \frac{S(r)}{4\pi r^2} \tag{3.31}$$

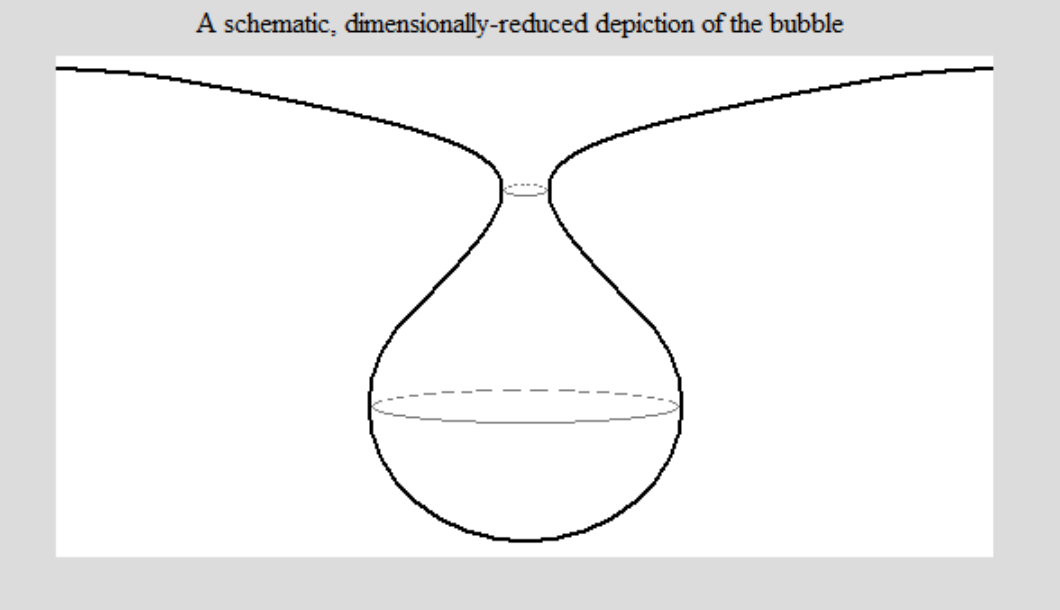

Figure 3.1: *A highly simplified representation of the manifold* $S^3 \# Sch^3$

and thus, in the notation of (3.2) we have $A(r) := A(r,0) = B(r,0) =: B(r)$, so

$$ds^2(t=0) = e^{2A(r)}\left(dr^2 + r^2 d\Omega^2\right) \tag{3.32}$$

The question then arises of whether this is in fact a two dimensional problem. If $A(r,t) = B(r,t)$ at $t = 0$, can we not simply factor $e^{2A(r,t)}$ out of the metric and start the flow, making this a one dimensional problem? At first, there does not seem to be a problem with this, but as soon as we start the Ricci flow, we see that if the above method was permissible, then our solution $g(t)$ would satisfy

$$2e^{2A}\frac{\partial A}{\partial t} = \frac{\partial g_{11}}{\partial t} = -2R_{11} \tag{3.33}$$

$$2e^{2A}\frac{\partial A}{\partial t} = \frac{\partial g_{22}}{\partial t} = -2R_{22} \tag{3.34}$$

This system has no solutions if R_{11} is not identically equal to R_{22}. This problem is solved by the DeTurck trick, and the resulting problem is indeed two dimensional. This justifies our use of two different functions, even though they are equal in the data we have specified.

3.5 Our Boundary Conditions and their Geometric Motivation

In sections 3.1−3.4 we dealt with the initial conditions. The initial conditions are defined by the question we want to ask − that is, they are defined by the

geometry that we want to flow. The question of boundary conditions is not quite as straightforward, especially for geometric PDEs such as the Ricci flow equation. We must choose boundary conditions such that the solution of the Ricci flow is, in fact, telling us something about the geometry in question, and this is not always easy. We have two boundaries to deal with: the origin, and the value r_{max}, which serves as "pseudo-infinity" in our numerical simulation.

At the origin, we want to tell the mathematics that we are dealing with part of a 3-sphere. This may seem to be implied by the initial conditions, but we need to say a bit more. If our boundary condition does not force $S(t, r = 0) = 0$, then this allows for $S(t, r = 0) > 0$, in which case the flow leads to a "hole" in the sphere at the origin[1], or $S(t, r = 0) < 0$, in which case the sphere is self-intersecting. This might suggest that we want a Dirichlet condition on $S(t, r)$ at the origin, namely $S(t, r) = 0$. But not so fast! We would also like the sphere to be smooth at the origin. If, for example, a cone point develops at the origin after any nonzero time, then the PDE is not representing the geometric flow we want to explore. If the geometry is smooth

[1]This is an issue with PDEs that are meant to represent something geometrical − it is easy to assume that "of course property X will hold," if one is picturing the manifold we intend to represent, rather than keeping in mind precisely which assumptions we are making in our model. After all, the development of a "hole" in the manifold at the origin is entirely consistent with the initial data we specified − the numerics do not know what we intend to represent.

at the origin, then by definition it is locally Euclidean, which means that we should have $S(t,s) \longrightarrow 4\pi s^2$ as $s \longrightarrow 0$, where s is arclength measured along the 3-surface. This implies that

$$\frac{\partial S}{\partial s} = 8\pi s = 0 \tag{3.35}$$

at $s = 0$. As such, it would seem that we also must enforce a Neumann condition at the origin. This is troubling, as we can only enforce one condition on S at the origin. Luckily, a particular boundary condition does the trick. We seek solutions that satisfy

$$Hs \longrightarrow 2 \quad \text{as} \quad s \longrightarrow 0 \tag{3.36}$$

where H is the mean curvature. This manifests itself in MATLAB as the Neumann condition mentioned above, and luckily, it also enforces the Dirichlet condition $S(t, r = 0) = 0$.

The boundary condition on $S(t,r)$ at r_{max} is the same as that used in [2]. This is justified since the geometry at infinity is the same in both cases (i.e., it is Schwarzschild). Written in geometric language, this condition is

$$H(t, r_{max}) = H(0, r_{max}) \tag{3.37}$$

where as before, $H(t,r)$ is the mean curvature.

The boundary condition on $A(t,r)$ in both cases is to set the DeTurck vector $X = 0$. At the origin, this is motivated by the rotational symmetry of

the problem and the requirement that the DeTurck vector field be smooth. The only way to force both of these conditions is to force $X = 0$. At the origin, this condition becomes $\frac{\partial A}{\partial r} = 0$, while at "infinity," the condition $X = 0$ becomes

$$e^{-2A(t,r_{max})}\big(\partial_r A - 2\partial_r B\big) - \left(\frac{2}{r_{max}}\right)\left(e^{-2A(t,r_{max})} - e^{-2B(t,r_{max})}\right) = 0 \quad (3.38)$$

Chapter 4

The Numerical Simulation of Ricci Flow

4.1 MATLAB's `pdepe` Routine

So far, we have described the general procedure of Ricci Flow, and the initial data from which we will be flowing. Unfortunately, as we discussed in section 2.5, it is extremely difficult to solve the Ricci Flow equation analytically in most cases. We can circumvent this problem by implementing a numerical simulation of Ricci Flow. In what follows, we will describe the numerical methods used to simulate Ricci Flow in MATLAB.

MATLAB's `pdepe` routine is designed to numerically solve initial-boundary value problems for elliptic and parabolic systems of PDEs in one space dimen-

sion. Thankfully, since our problem is rotationally symmetric, our three space dimensions can be reduced to one.

The `pdepe` routine is capable of solving systems of PDEs in which each equation of the system can be written in the following form:

$$c(x,t,u,\partial_x u)\frac{\partial u}{\partial t} = x^{-m}\frac{\partial}{\partial x}\Big(x^m f\left(x,t,u,\partial_x u\right)\Big) + s\left(x,t,u,\partial_x u\right) \tag{4.1}$$

The constant m is determined by the symmetries of the PDE, and can take the values 0, 1, or 2, representing no symmetry, cylindrical symmetry, and spherical symmetry respectively. Although our problem is concerned with a geometry that displays a great deal of symmetry, we have suppressed redundant dimensions before coding the PDE into MATLAB, and so our equation has $m = 0$, corresponding to no symmetry.

To use `pdepe`, we must feed it two lattices, called xmesh and tspan. These are discretizations of space and time respectively, and they are used quite differently by the routine.

As for tspan, time integration is accomplished in `pdepe` using `ode15s`, one of MATLAB's many ODE solvers. This ODE solver dynamically adapts both its time discretization and its update formula. As such, our choice of tspan does not matter much for purposes of computation. The number of points we choose to allocate to tspan weakly determines the "effort" that `pdepe` will put into the computation, and the relative clustering of those points weakly

determines which areas `pdepe` will focus its effort on, with areas of rapid change "earning" more of the lattice points than other areas, all else being equal.

The vector xmesh is considerably more important, and it will serve as the lattice on which space is discretized and on which second order approximations to the exact solution are computed. Unlike tspan, the total points and their relative clustering in xmesh strongly determine the total cost and relative importance of those points in the computation. Clustering is desirable in regions where the solution changes very quickly.

For reasons that are beyond the scope of our discussion, `pdepe` must often perform fairly complicated adjustments of the initial parameters for certain equations, especially elliptic PDEs. Fortunately, such adjustments are not required for parabolic equations, such as our Ricci-DeTurck equation. This is one of several considerations that make `pdepe` well suited for our problem. For more details on the `pdepe` routine, see the MathWorks documentation [14].

4.2 What we're simulating

For the sake of completeness, in this section we include a complete summary of the system of PDEs we will be simulating numerically, as well as our initial data, and boundary conditions.

Our PDEs are:

$$\frac{\partial A}{\partial t} = e^{-2A}\left(\frac{\partial^2 A}{\partial r^2} - \left(\frac{\partial A}{\partial r}\right)^2 + \frac{1}{2S^2}\left(\frac{\partial S}{\partial r}\right)^2\right) \tag{4.2}$$

$$+\frac{8\pi r^2}{S}\left(\frac{1}{r}\frac{\partial A}{\partial r} - \frac{1}{rS}\frac{\partial S}{\partial r} + \frac{1}{r^2}\right)$$

$$\frac{\partial S}{\partial t} = e^{-2A}\left(\frac{\partial^2 S}{\partial r^2} - \frac{1}{S}\left(\frac{\partial S}{\partial r}\right)^2\right) + \frac{8\pi r}{S}\frac{\partial S}{\partial r} - 8\pi \tag{4.3}$$

Our initial conditions are:

$$A(0,r) = \begin{cases} \log\left[\frac{1}{4}\left(1+\frac{1}{r}\right)^2\right] & : r \in [r_J, \infty) \\ \\ \log\left[\frac{1}{4}\frac{\left(1+r_J^{-1}\right)^3}{\left(1+(r^2/r_J^3)\right)}\right] & : r \in (0, r_J] \end{cases}$$

$$S(0,r) = \begin{cases} \frac{\pi r^2}{4}\left(1+\frac{1}{r}\right)^4 & : r \in [r_J, \infty) \\ \\ \frac{\pi r^2}{4}\frac{\left(1+r_J^{-1}\right)^6}{\left(1+(r^2/r_J^3)\right)^2} & : r \in (0, r_J] \end{cases}$$

And finally, our boundary conditions on $S(t,r)$ are:

$$Hs \longrightarrow 2 \quad \text{as} \quad s \longrightarrow 0 \tag{4.4}$$

and

$$H(t, r_{max}) = H(0, r_{max}) \tag{4.5}$$

while our boundary condition on $A(t,r)$ at both endpoints is to set the DeTurck vector $X = 0$.

4.3 A Stumbling Block: The Spike Singularity

In this section, I will briefly describe an singularity that arose in the course of the simulations, in the hope that it may save some time for others who wish to pursue the application of numerical techniques to the study of Ricci flow. Early in the simulations, we noticed that the plot of $A(t,r)$ seemed to develop a tall, thin "spike" at the origin, despite the fact that the "$X = 0$ at $r = 0$" boundary condition forced $\frac{\partial A}{\partial r} = 0$. Eventually, I was able to localize the source of the spikes to three terms in the PDE for $A(t,r)$. The PDE for $A(t,r)$ is:

$$\frac{\partial A}{\partial t} = e^{-2A}\left(\frac{\partial^2 A}{\partial r^2} - \left(\frac{\partial A}{\partial r}\right)^2 + \frac{1}{2S^2}\left(\frac{\partial S}{\partial r}\right)^2\right) \tag{4.6}$$
$$+\frac{8\pi r^2}{S}\left(\frac{1}{r}\frac{\partial A}{\partial r} - \frac{1}{rS}\frac{\partial S}{\partial r} + \frac{1}{r^2}\right)$$

Since the problem occurs at the origin, we need to examine the behavior of this PDE near the origin. To do so, it will prove to be helpful to rewrite the equation in terms of arclength. The arclength, measured along the manifold, from the "origin" to a point with coordinate r is

$$s(t,r) = \int_0^r e^{A(t,r')}dr' \tag{4.7}$$

And so

$$\frac{\partial s}{\partial r} = e^{A(t,r)} \tag{4.8}$$

Moreover, we have

$$s \longrightarrow re^{A(t,0)} \quad \text{as} \quad r \longrightarrow 0 \tag{4.9}$$

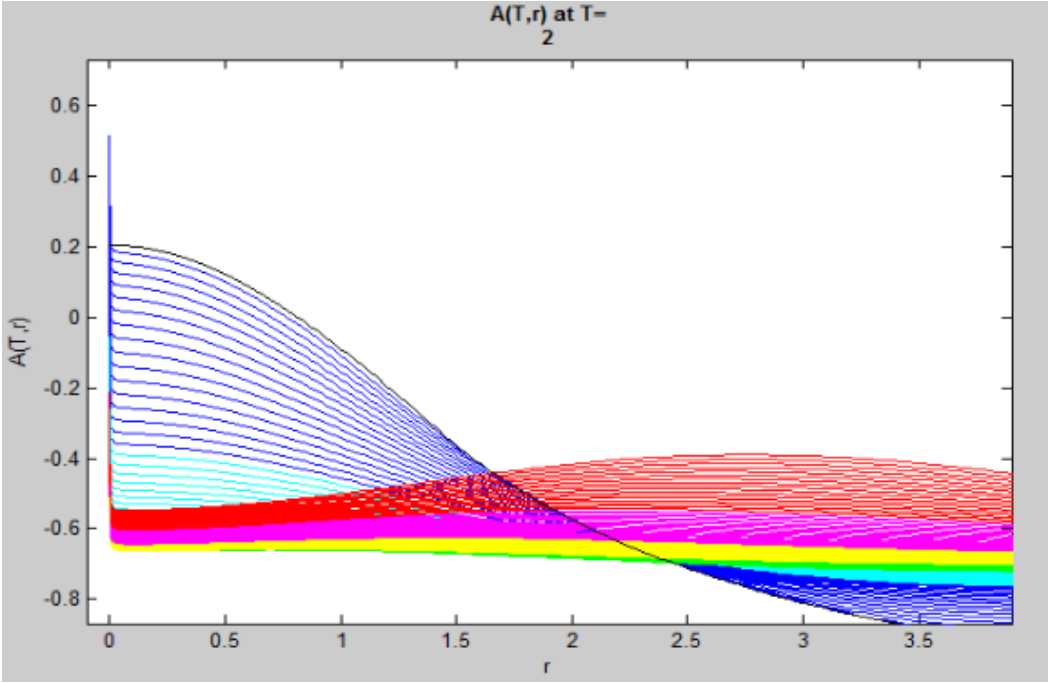

Figure 4.1: *An example of the spike singularity. The derivative should be zero at the origin, but instead we see a rapid increase. Each curve represents* $A(t, s)$ *for a fixed time, and different curves represent different times. The passage from blue to red corresponds to the direction of increasing time. See chapter 5 for a more complete discussion.*

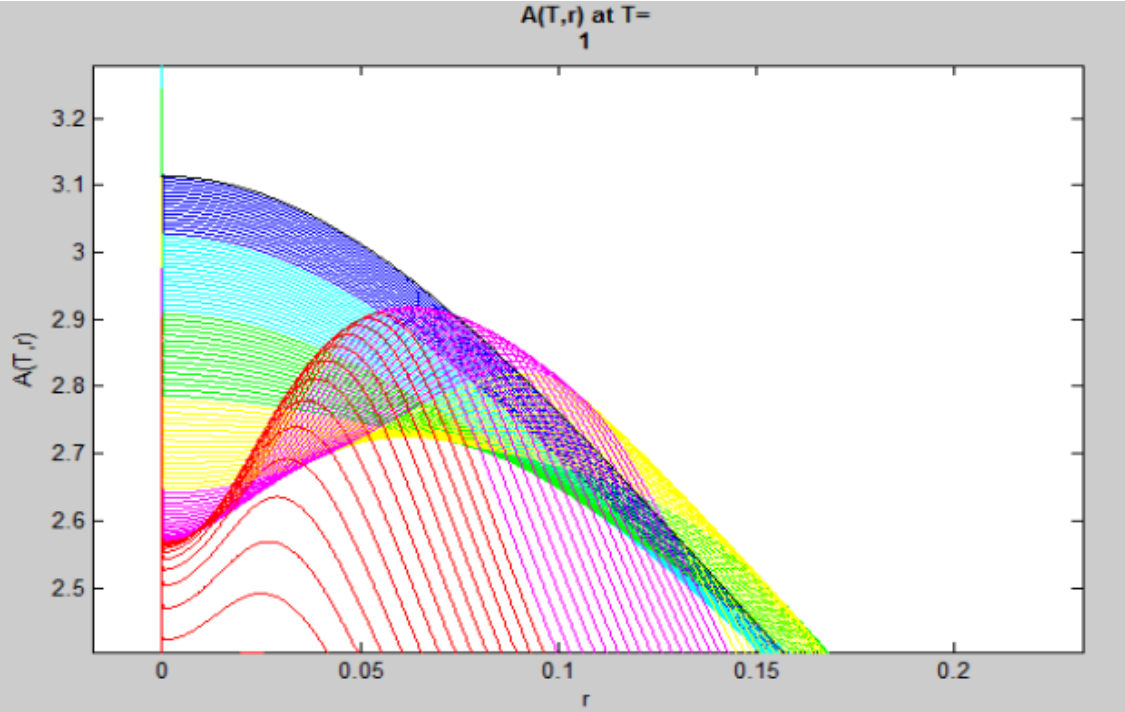

Figure 4.2: *A close-up of the spike singularity.*

This lets us rewrite (4.2) near $r = 0$ as:

$$\frac{\partial A}{\partial t} = \frac{\partial^2 A}{\partial s^2} - \left(\frac{\partial A}{\partial s}\right)^2 + \frac{1}{2S^2}\left(\frac{\partial S}{\partial s}\right)^2 + \frac{8\pi s}{S}\left(\frac{\partial A}{\partial s} - \frac{1}{S}\frac{\partial S}{\partial s} + \frac{1}{s}\right) \tag{4.10}$$

Since our boundary conditions force the bubble to be locally Euclidean at the origin, we have

$$\frac{S(t,s)}{4\pi s^2} \longrightarrow 1 \quad \text{as} \quad s \longrightarrow 0 \tag{4.11}$$

Now, notice the behavior of the 3rd, 5th, and 6th terms to the right of the equality in (4.10) as we replace $S(t,s)$ with $4\pi s^2$. They become

$$\frac{1}{2S^2}\left(\frac{\partial S}{\partial s}\right)^2 - \frac{8\pi s}{S^2}\frac{\partial S}{\partial s} + \frac{8\pi}{S} \tag{4.12}$$

$$= \frac{(8\pi s)^2}{2(4\pi s^2)^2} - \frac{(8\pi s)^2}{(4\pi s^2)^2} + \frac{2}{s^2} \tag{4.13}$$

$$= \frac{2}{s^2} - \frac{4}{s^2} + \frac{2}{s^2} = 0 \tag{4.14}$$

This leads to a singularity that anyone conducting a numerical simulation of Ricci flow on a complete manifold with an origin of symmetry should look out for. The problem results from the fact that, although these three terms cancel exactly as $s \longrightarrow 0$, *any* error in the computation of $S(t,s)$ and $\partial_s S$ can easily lead to an error in the coefficients 2, -4, and 2 in equation 4.14. However, a small error in the coefficients does not lead to a small error in the result, since for all $\epsilon_i > 0$

$$= \frac{2+\epsilon_1}{s^2} - \frac{4+\epsilon_2}{s^2} + \frac{2+\epsilon_3}{s^2} = \frac{\epsilon_1 - \epsilon_2 + \epsilon_3}{s^2} \longrightarrow \infty \quad \text{as} \quad s \longrightarrow 0 \tag{4.15}$$

unless we happen to be infinitely lucky and the errors cancel, which they generally do not. This was the source of the "spike" singularity. It is often difficult to identify the source of such numerical instabilities, and to subsequently fix them. As such, we discuss this singularity in the hope that it might help others who wish to pursue numerical simulations of Ricci flow. The singularity problem can be solved as follows. If we expand S near the origin by

$$S(t,s) \approx 4\pi s^2 + c(t)s^4 \tag{4.16}$$

then we see that the three terms in (4.12) do not cancel exactly, but rather that they sum to $\frac{c(t)}{4\pi}$. It remains to figure out what $c(t)$ is. Plugging this expansion into the PDE for $S(t,s)$ gives an ODE for $c(t)$, which can easily be solved to give $c(t) = 0$. Therefore, we can remove the spike singularity by manually setting

$$\frac{1}{2S^2}\left(\frac{\partial S}{\partial s}\right)^2 - \frac{8\pi s}{S^2}\frac{\partial S}{\partial s} + \frac{8\pi}{S} = 0 \quad \text{as} \quad s \longrightarrow 0 \tag{4.17}$$

This is accomplished by setting the above term equal to zero for the first 1 or 2 points in the spatial lattice. Notice that we are simply setting this term equal to the value that it is manifestly equal to at $s = 0$. As such, we are not changing either the problem or the PDE, but simply forcing the numerics to behave as they should.

Chapter 5

Our Results

5.1 Ricci-DeTurck flow of the bubble

The following section explores the numerical simulation of the Ricci-DeTurck flow, as applied to the bubble, for various values of the geometric parameter

$$k^2 = \frac{S\left(H^{-1}\left(0\right)\right)_{S^3}}{S\left(H^{-1}\left(0\right)\right)_{Sch^3}} = \frac{\text{Area of } S^3 \text{ equator}}{\text{Area of } Sch^3 \text{ throat}} \tag{5.1}$$

We first analyze the Ricci-DeTurck flow of the initial data discussed in chapter 3. Our goal is to determine whether there exist values of k^2 for which the flow exists for all time, whether there are some "regions of collapse" in which the metric becomes singular after some finite time, and in each case to obtain an approximation of these values.

As we discussed in the introduction, the metric we examine here may be thought of as an intermediate case between Garfinkle and Isenberg's corseted

spheres [8], which displayed threshold behavior, and Balehowsky and Woolgar's $\mathbb{RP}^3$ Geon [2] which flows to a singular metric as the neck collapses for all parameter values.

In the case of the Ricci-DeTurck flow, it suffices to examine the bubble in the case of a stable minimal surface. By a stable minimal surface, we mean a closed surface whose area is less than that of any neighboring closed surface. This is possible thanks to a result of Oliynyk and Woolgar [18], which proved that the flow of the bubble exists for all $t > 0$ when there is no minimal surface.

Figure 5.1 is an illustration of the flow for $k^2 = 2$, using $S(t, s)$ to study collapse. Recall that the function $S(t, s)$ represents area as a function of arclength measured from the origin, at time t. Each line on the plots below is the graph of $S(t, s)$ at a given time, with different lines representing different times. Dark blue lines correspond to times near $t = 0$, red lines represent times near the end of the time interval examined in a given plot, and intermediate colors represent intermediate times. The passage from "cool" colors (e.g., blue, green) to "warm" colors (e.g., yellow, red) is thus the direction of increasing time[1]. Although the meaning of $S(t, s)$ is more geometrically transparent, we also plot $A(t, s)$ in figure 5.2 to give an overall flavor of the evolution.

Plotting $S(t, s)$ versus arclength gives us a reasonably accurate picture of

[1]This visualization method allows for the comparison of the flow at different times, in a way that standard 3-D plots often obscure on paper, when one cannot actively rotate the plot to gain perspective.

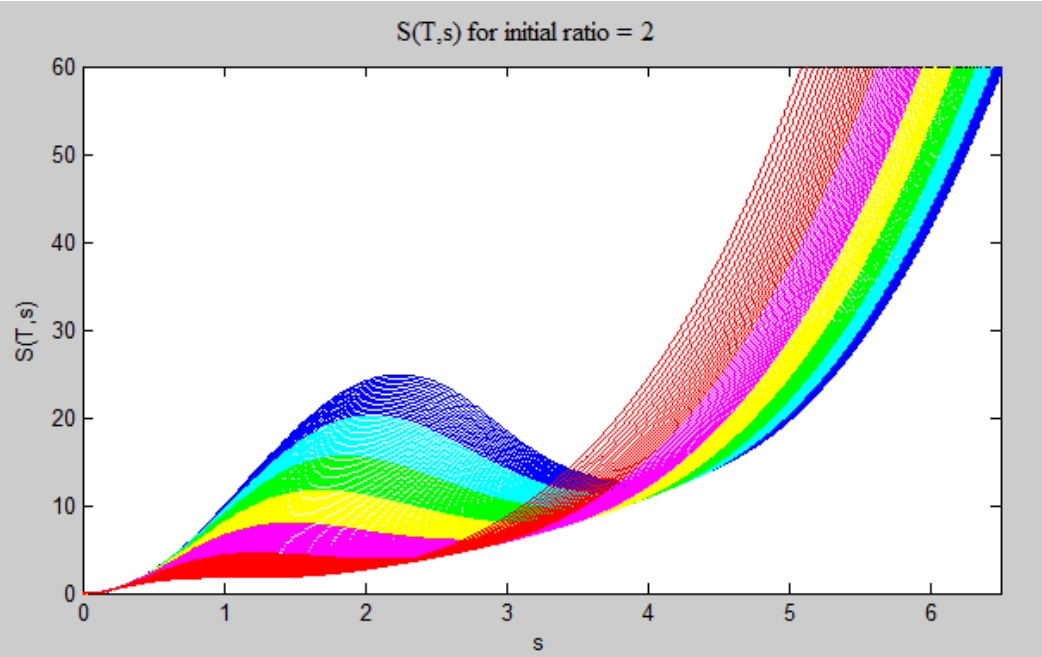

Figure 5.1: *The evolution of $S(t, s)$ for the Ricci-DeTurck flow of the bubble when $k^2 = 2$. We have cropped the picture for easy viewing, but the curves in this data set have rMax = 10 (as do all plots of $S(t, s)$ in the various cases below) and continue up to approximately $S(t, s) = 130$. The direction from blue curves through green, yellow and finally red represents the passage of time from the initial data onward, respectively.*

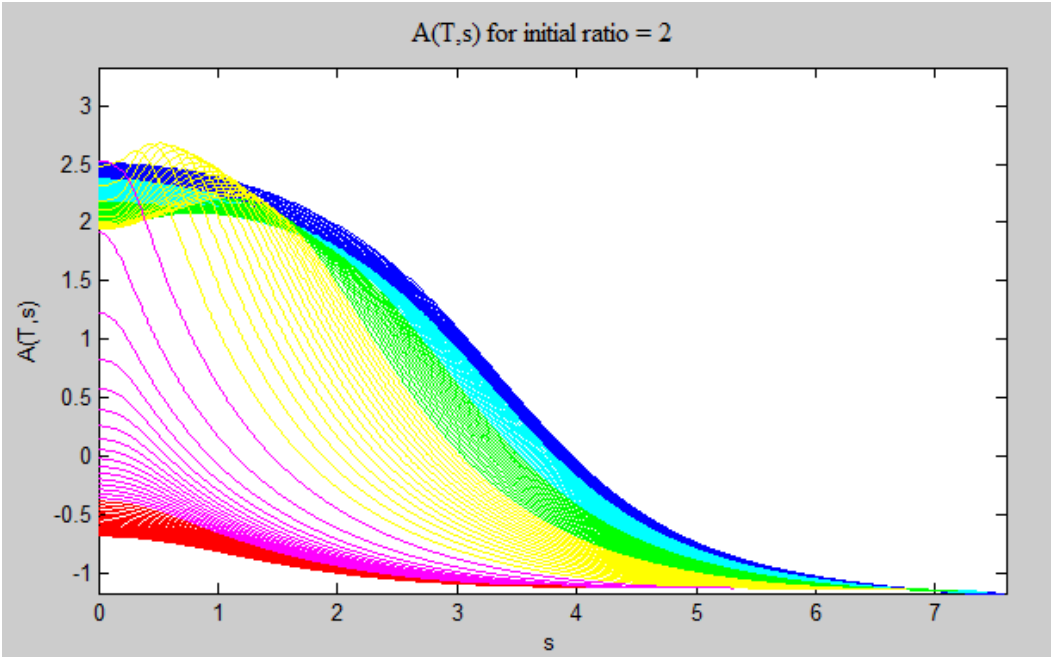

Figure 5.2: *The evolution of $A(t, s)$ for the Ricci-DeTurck flow of the bubble when $k^2 = 2$*

what the flow looks like after suppressing angular dimensions. It is apparent that for $k^2 = 2$, the minimal surface eventually disappears. The simulations therefore suggest that there is a region, at least those values of $k^2 \in [1, 2]$, such that the bubble flows to a metric without a minimal surface. From that point on, the flow exists and converges to flat $\mathbb{R}^3$ as $t \longrightarrow \infty$ [18].

Now, we will explore the following question: Is there a region in which the flow collapses the manifold at the throat? Since we are examining the issue numerically, it is less straightforward to establish collapse than it is to establish the disappearance of the minimal surface. This is due to the face that as the manifold collapses, the curvature becomes very large near the throat. For a fixed number of points in the spatial discretization, as the curvature becomes very large, the plots eventually develop "kinks," no matter how many points we include in the spatial lattice. When such kinks have developed, we are no longer justified in trusting the numerics. An example of this type of situation is pictured in figure 5.3 for $k^2 = 3$. However, we can still get strong evidence of collapse before the kinks form. It is a sufficient, though not necessary, condition for collapse that $k^2(t)$ is an increasing function of time. If $k^2(t)$ is *eventually* increasing for a given initial value of $k^2 := k^2(0)$, then this would provide reasonable evidence that the flow becomes singular for this value of k^2. Figure 5.4 is the function of time $Ratio(t) = S(t, r_{equator})/S(t, r_{throat})$ for an initial ratio of 3: We see in figure 5.4 that the ratio starts at 3, and then

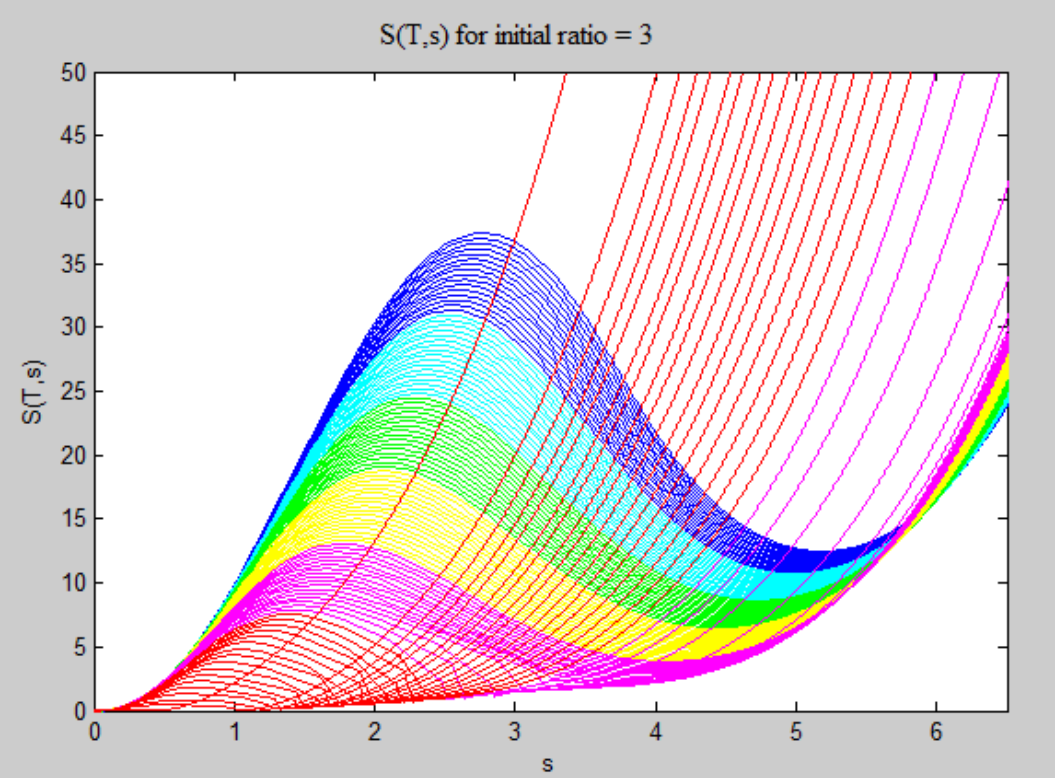

Figure 5.3: *The development of kinks in the Ricci-DeTurck flow when* $k^2 = 3$. *Notice that the code becomes unreliable at roughly the point of transition from the pink curves to the red curves.*

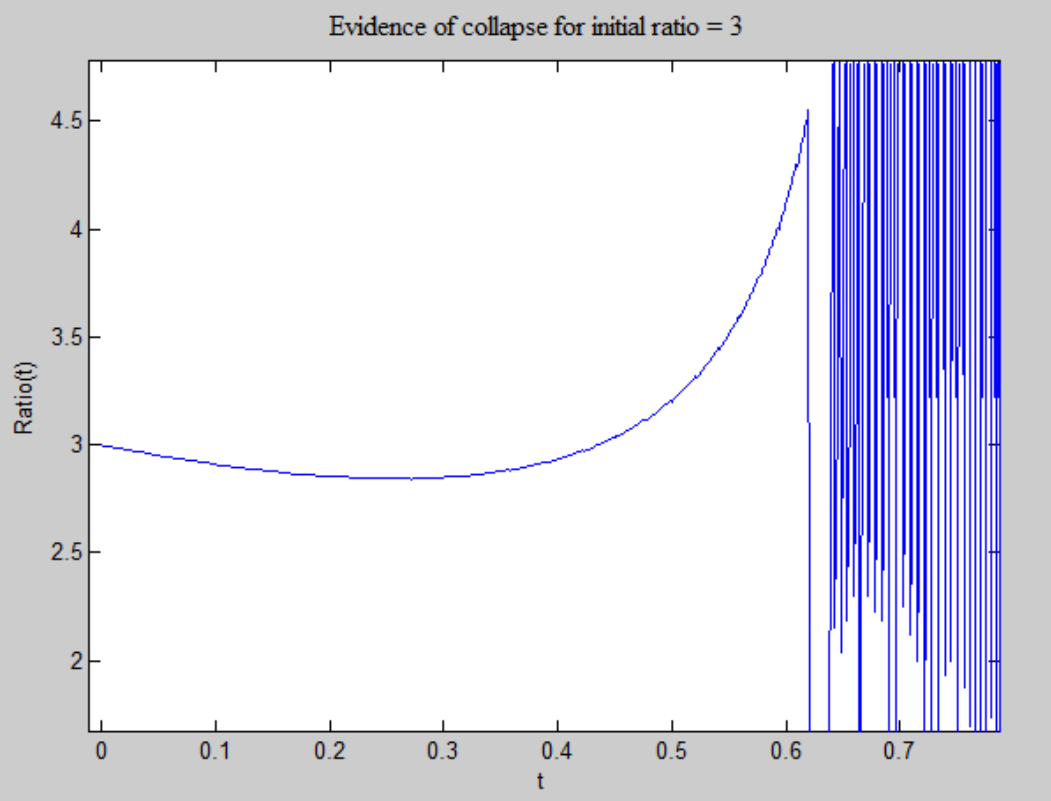

Figure 5.4: *Plotting Ratio*(t) *for* $k^2 = 3$ *shows strong evidence of collapse*

decreases for a short period. This decrease is an initial "breathing in" of the throat (i.e. a small decrease in $Ratio(t)$ for short times) that can be seen for all initial values of the ratio. However, the ratio soon begins to increase, and at an increasing rate, until the code becomes unreliable as kinks form at approximately $t = 0.62$. The data to the right of the point $t = 0.62$ can be discarded, as good evidence of collapse can be obtained before the point of breakdown.

Because this function is increasing before breakdown (as is its derivative), we may expect it to increase for the short additional time required to reach singularity formation. Remember that we do not need to extrapolate very far: as soon as the "throat" collapses to zero, the flow stops existing (even analytically), and the graphs above suggest that this collapse is happening rather quickly. An alternative that could throw a wrench into this argument, namely that the throat asymptotes to zero but never reaches it, is highly unlikely. Ricci flow tends to lead, fairly quickly, to the collapse of spheres and their products with intervals, namely ϵ-necks, as we discussed in section 2.5. We are therefore confident that certain values of k^2 lead to collapse for this 1-parameter family of geometries, while other values lead the geometry to flow indefinitely and to approach a smooth, "canonical" metric.

Our simulations suggest that the critical value of the area ratio for the Ricci-DeTurck flow lies somewhere in the neighborhood of $k^2 \approx 2.2$, although

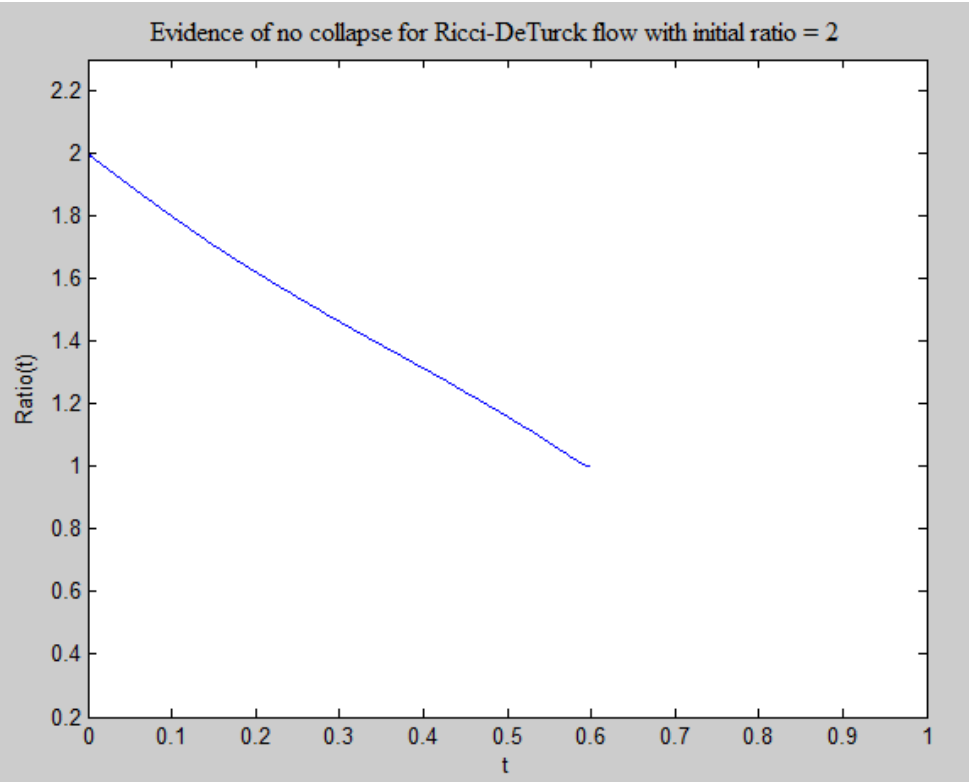

Figure 5.5: *Plotting* $Ratio(t)$ *for* $k^2 = 2$ *shows that this geometry does not collapse. The plot stops existing at roughly* $t = 0.6$ *as the minimal surface disappears.*

the methods we employ do not allow us a great degree of precision in pinpointing this value. Regardless, there exist values of k^2 for which the manifold flows smoothly to flat $\mathbb{R}^n$, and values for which the flow becomes singular. Figures 5.5 and 5.6 show the evolution of $Ratio(t)$ for $k^2 = 2$ and $k^2 = 2.3$. Notice that in the $k^2 = 2$ case, we get smooth evolution until roughly $t = 0.6$, at which time $Ratio(t) = 1$, and thereafter ceases to exist as the minimal surface disappears. In the $k^2 = 2.3$ case, notice that $Ratio(t)$ never descends below 1.5 (before breakdown), and starts to increase at roughly $t = 0.58$.

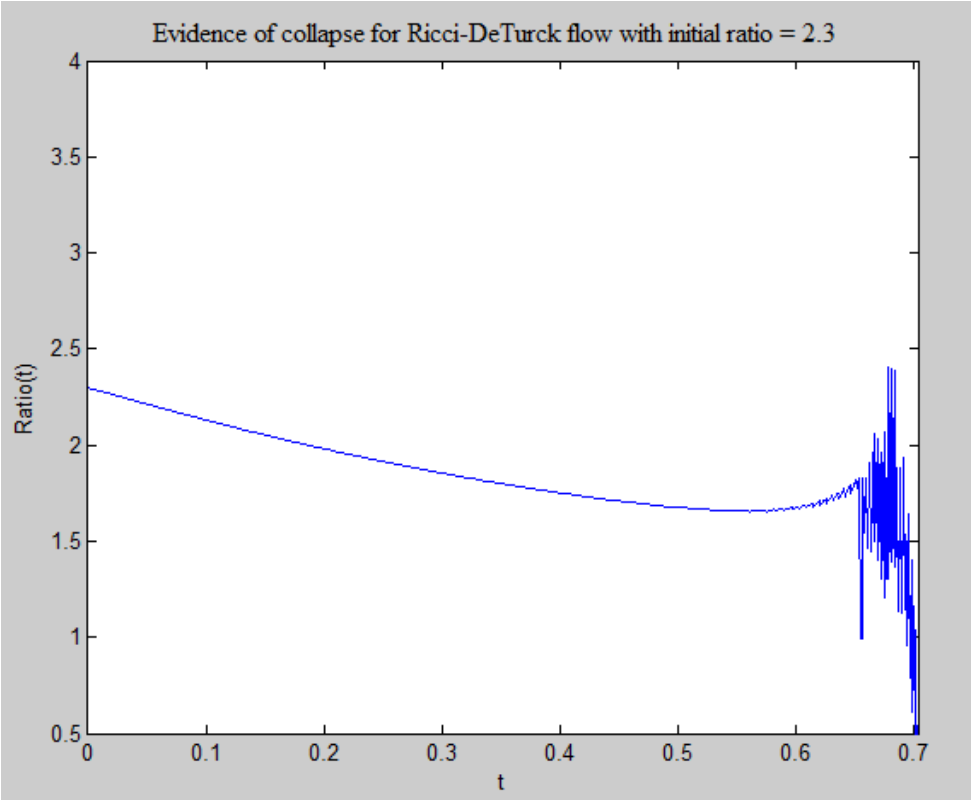

Figure 5.6: *Plotting Ratio*(t) *for* $k^2 = 2.3$ *shows that this geometry collapses before the point at which the code becomes unreliable near* $t = 0.65$

This suggests that the behavior displayed by Garfinkle and Isenberg's corseted spheres is neither a quirk of their particular choice of geometry, nor specific to compact manifolds per se. Rather, this aspect of the flow of 1-parameter families seems to be a general feature of Ricci flow. We expect that there exists a value of k^2 for which the geometry exhibits critical behavior, similar in character to Garfinkle and Isenberg's "javelin" geometry, but simulations thus far have not been able to address this question. The numerical evidence therefore strongly suggests that the Ricci flow on asymptotically flat $\mathbb{R}^n$ does not in general exist for all time.

Now, how does our value of $k^2 \approx 2.2$ compare to Garfinkle and Isenberg's value? In their original paper on the topic [8], they measured the degree of corseting using a parameter λ, whose critical value was found to be approximately $\lambda = 0.1639$. Conveniently, it turns out that $k^2 = \lambda^{-1}$, which puts their value of collapse at $k^2 \approx 6.10$ in our notation. Our results, therefore, imply that the bubble family collapses "more easily" (i.e. for smaller values of k^2, and thus less "pinched" minimal surfaces) than the family of corseted spheres. This result makes a great deal of sense if we think of the bubble, like before, as an intermediate case between Garfinkle and Isenberg's corseted spheres [8] and Balehowsky and Woolgar's $\mathbb{RP}^3$ geon [2]. We can summarize, in condensed form, how our result fits nicely between these two results as follows:

Schwarzscild on both sides is too much − it always collapses; 3-spheres on

both sides can collapse, but only with a lot of effort (i.e., once $k^2 \geq 6.10$); Schwarzschild on one side and a 3-sphere on the other may or may not collapse, as in the latter case, but the Schwarzschild side makes collapse easier to achieve, as expected from the former.

5.2 The List-DeTurck Flow of the bubble

We now examine the List flow of the bubble (See section 2.6 for a discussion of the List flow). In this section, we begin by focusing on the case of the bubble without a minimal surface, and we will numerically explore questions similar to those that were explored analytically in [10]. In the latter part of this section, we examine the List flow of the bubble with a stable minimal surface, and compare this flow's behavior to the Ricci-DeTurck case.

Since the fixed points of the List flow give solutions to the static Einstein equations, it is of considerable importance that the flow converge to those few fixed points that exist. That is, we might hope that we could start the flow at a more or less arbitrary initial geometry and flow to some fixed point or another, without the flow stopping due to singularity formation along the way. Long-time existence of the List flow in various cases is thus an important question. Because of this, the first question we will examine is a question of long-time existence: does the addition of the scalar field cause the List flow to collapse in cases when the Ricci-DeTurck flow would exist for all time? We will

examine the List flow of the bubble for the critical value $k^2 = 1$, a value for which the bubble is as close as it can be to having a minimal surface. We know that the Ricci flow of this geometry exists for all time. Does the added scalar field in List's flow cause the throat to collapse? This question was addressed analytically in [10], and plots 5.7− 5.9 and 5.15 below appear to justify an assumption by Gulcev, Oliynyk, and Woolgar (as do as all simulations not pictured). In [10], the authors showed analytically the long-time existence of the rotationally symmetric List flow in the case of no minimal surface, but their argument required the strong and undesirable assumption that there exists a function $f(t) : [0, \infty) \to \mathbb{R}$, such that

$$\frac{|\nabla u|}{r} \leq f(t) \tag{5.2}$$

for the duration of the flow. As such, if the flow only exists for $t \in [0, T)$, then $\frac{1}{r}|\nabla u| \leq \sup_t f(t)$. Equivalently, the assumption may be expressed by saying that $\frac{1}{r}|\nabla u|$ is allowed to blow up, but not in finite time. The results of our numerical simulations suggest that the List flow exists for all $t > 0$ in the absence of any such assumption. For example, the List flow of the bubble with initial scalar field $u(0, r) = A \sin(r) e^{-r^2}$ where A is constant satisfies

$$\frac{1}{r}|\nabla u| = A e^{-r^2} \frac{|\cos(r) - 2r \sin(r)|}{r} \longrightarrow \infty \quad \text{as} \quad r \longrightarrow 0 \tag{5.3}$$

Yet our simulations suggest that the flow of this geometry exists for all time, as we will see at the end of section 5.3. However, this only obliquely addresses

the question of whether the assumption of Gulcev, Oliynyk, and Woolgar is required. The assumption they required was that if one's initial data satisfies 5.2, then so does the flow for the rest of the time that it exists. In that sense, the initial scalar field $u(0, r) = A\sin(r)e^{-r^2}$ is even nastier than we strictly need to test Gulcev et al's assumption. Even so, the sectional curvatures for this data smooth-out immediately (although they begin at infinity). This is cause for optimism. If even such nasty data appears to become smooth and stay smooth, then it appears that Gulcev et al's weaker assumption may be justified.

Figures 5.7– 5.9 show the evolution of $S(t, s)$, $A(t, s)$, and the scalar field $u(t, s)$ under the List flow. In these plots, we begin with an initially Gaussian scalar field with an amplitude of 0.3 and a width of 0.1, though qualitatively similar behavior was observed for all parameter values explored to date. The single black curve in each plot represents that function's initial condition: We can see that the addition of the scalar field does not, even for short times, lead to the development of a minimal surface, in agreement with Theorem 1.3 of [10]. The flow appears to exist for all time, and the function $S(t, s)$ converges fairly rapidly to $4\pi s^2$. That is to say, the geometry of the bubble converges to $\mathbb{R}^3$ with the flat metric.

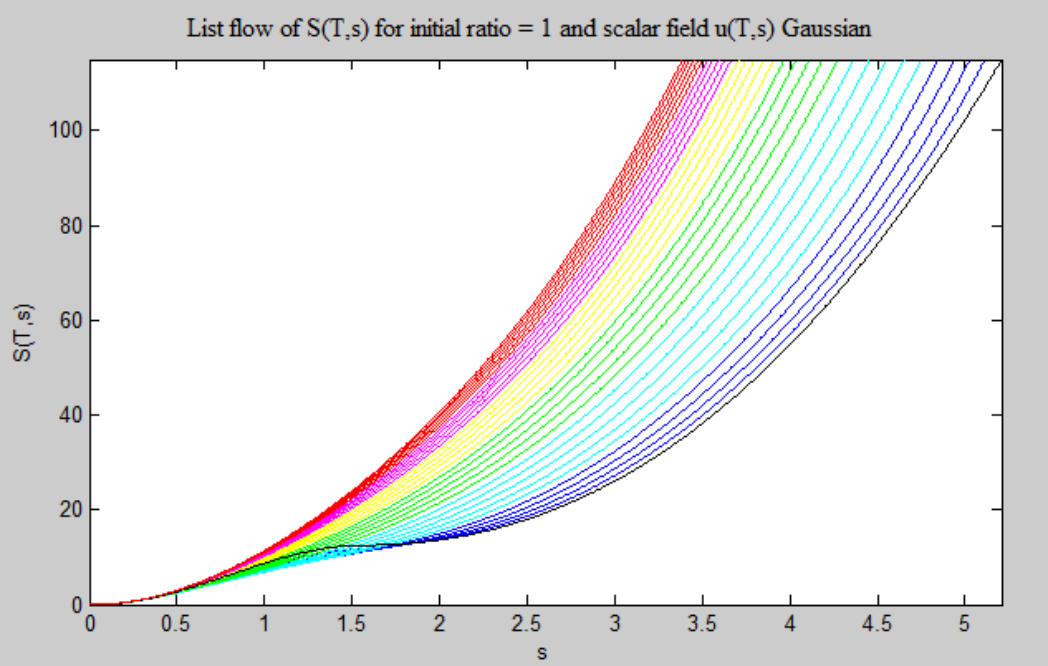

Figure 5.7: *The evolution of $S(t, s)$ for the List flow of the bubble. Recall that the change from blue curves to green, yellow and red represents the passage of time from the initial data onward, respectively.*

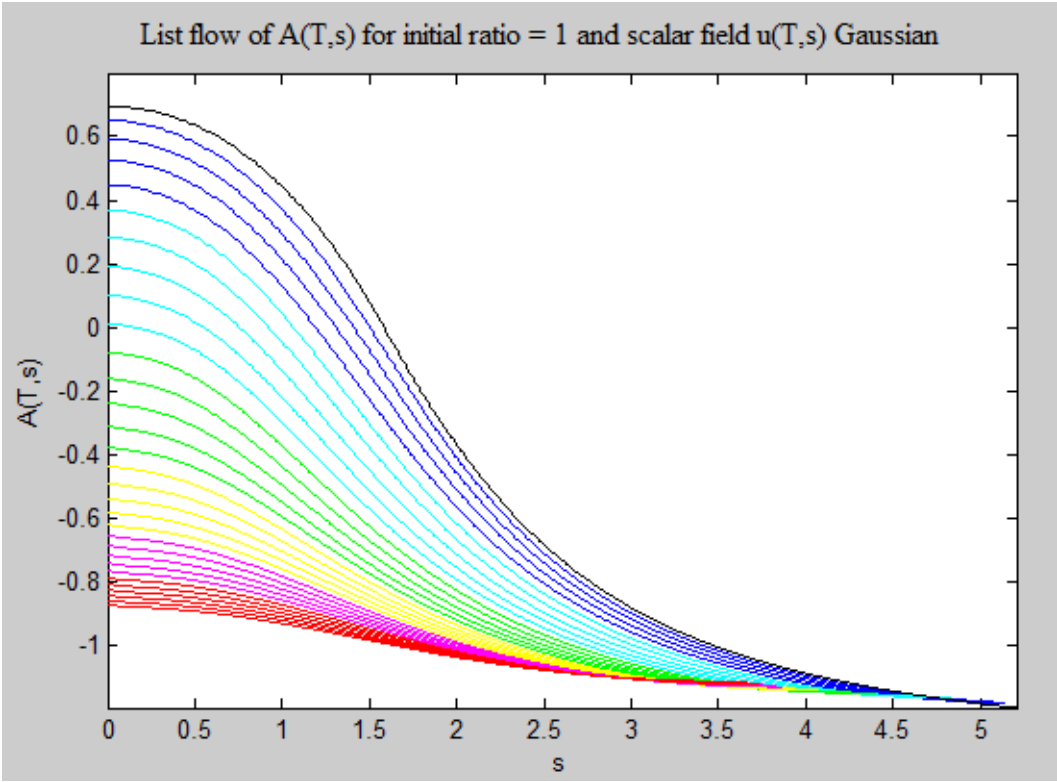

Figure 5.8: *The evolution of $A(t, s)$ for the List flow of the bubble*

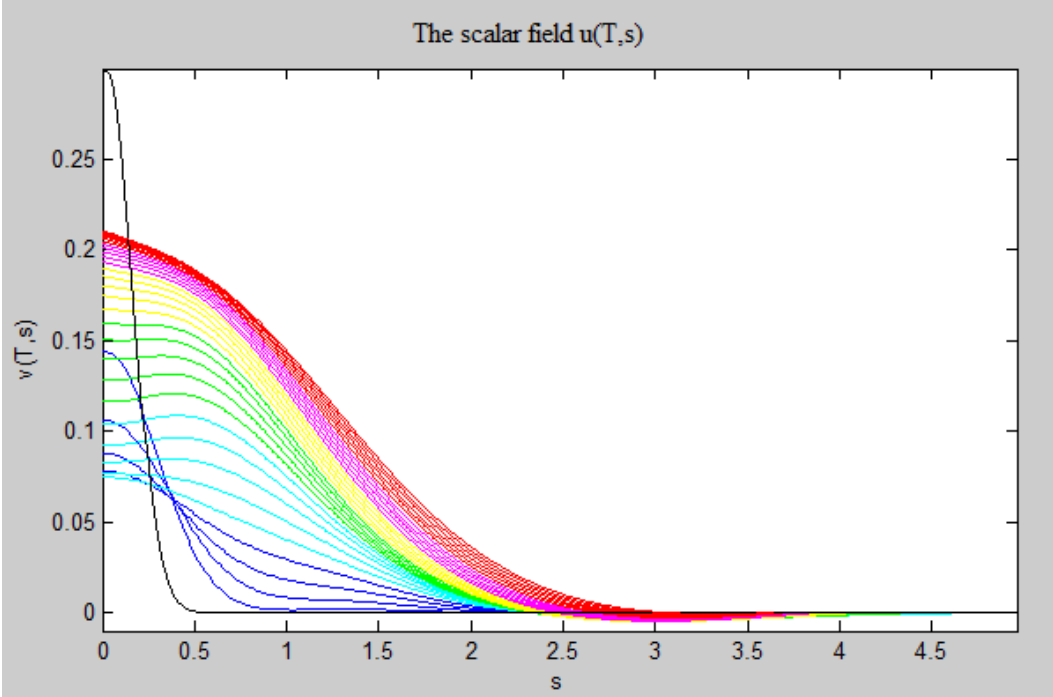

Figure 5.9: *The evolution of* $u(t, s)$ *for the List flow of the bubble*

5.3 Long Time Existence and Sectional Curvature

By examining the plots above, we concluded that the List flow seems to exist for all time when no stable minimal surface is initially present, and that the bubble flows to flat $\mathbb{R}^3$. However, in our explorations of the Ricci-DeTurck flow in section 5.1, we found that the numerics continued to generate data, even after the point at which the simulation was no longer reliable. We can easily notice the breakdown of numerical reliability in the case of the collapse of the bubble at the throat, but we would like to be sure that there are not other causes, perhaps more subtle and less easily detectable, of numerical breakdown. One such possibility suggests itself: perhaps the List flow does not, in fact, exist for all time, due to the development of a cone point at the origin. Such a cone point may go undetected by the analysis above, which focused on the long-time qualitative behavior of $S(t, s)$, $A(t, s)$, and $u(t, s)$. If such a point develops, though, this would prevent the long-time existence of the List flow, and in turn prevent the extraction from the flow of a fixed point and thus a solution to the static Einstein equations. The main concern in this case is *not* the fixed point itself, nor the spacetime which we could construct from it. After all, if the above simulations are accurate, then the fixed point is trivial – it is simply flat $\mathbb{R}^3$. Rather, the goal is to understand the long-time behavior

of the List flow in various cases (e.g., Is the development of cone points a generic feature of the flow for rotationally symmetric geometries? Is long-time existence generally very difficult to achieve?), in order that we might apply the intuition thus gained to geometries from which the extraction of a nontrivial solution to the Einstein equations is feasible. To answer some of these questions for the List flow of the bubble, it suffices to examine the sectional curvatures at the origin. If a cone point develops but is undetectable by the above methods, then we should be able to see evidence of it in the divergence of the sectional curvatures at the origin for long flow times. That is, the sectional curvatures should blow up if a cone point develops. Figure 5.10 shows that this is not the case. Although the sectional curvatures grow slightly after we turn on the flow, they soon dive toward zero. These sectional curvatures, together with the plots of $S(t, s)$, $A(t, s)$, and $u(t, s)$ above, provide strong evidence that the List flow in this case exists for all time, and eventually converges to $\mathbb{R}^3$ with the flat metric. Note, figure 5.10 shows the sectional curvature in any plane in the tangent space containing $\frac{\partial}{\partial r}$. The plot of the sectional curvature in planes tangent to the S^2 orbits of the rotational symmetry is not shown, because it turns out to be identical (at least at the origin, which is the point of interest).

Now, what about the List flow of the bubble with a stable minimal surface? We know that the addition of the List scalar field does not cause a minimal surface to form if we flow from initial data that is "infinitely close" to having

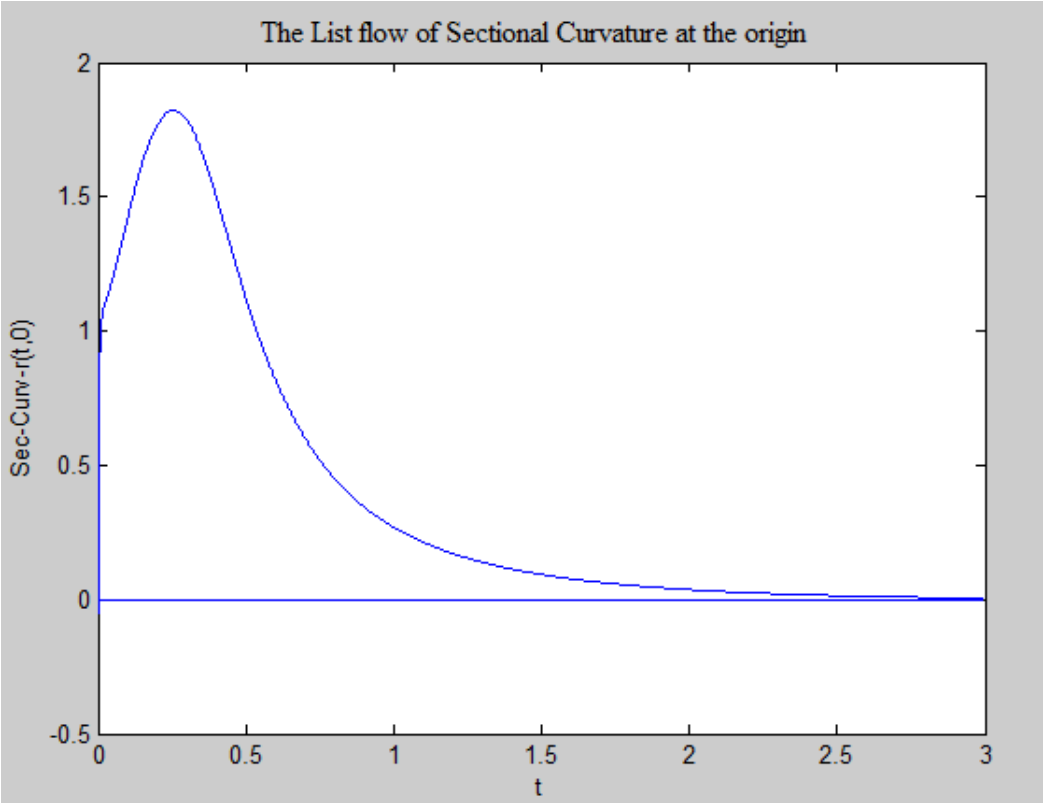

Figure 5.10: *The List flow of the sectional curvatures at* $r = 0$.

a minimal surface – that is, initial data with $k^2 = 1$. The first question that arises is whether the addition of the scalar field tends to "push" the bubble toward collapse, or away from it. That is, does there exist a value of k^2 for which the List flow and the Ricci-DeTurck flow exhibit different long-time qualitative behavior? If so, in which direction is the difference? Our simulations show that there is indeed an effect of the scalar field, and it seems to push the geometry *toward* collapse. As an example, figures 5.11 and 5.12 show the evolution of $Ratio(t)$ in the Ricci-DeTurck flow and the List flow for $k^2 = 2$. The scalar field for the List flow was a Gaussian with an amplitude of 3 and a width of 0.1, though this behavior does not sensitively depend on these particular parameter values. That is, although the size of the scalar field (both in terms of its amplitude and its width) certainly influences collapse, we did not have to finely tune the parameters to those values depicted in our examples to get these results; the results appear to hold quite generally. In both plots, we begin with the same geometry: the bubble with initial ratio $k^2 = 2$. In the first plot, the ratio steadily decreases until the time $t \approx 0.6$, at which point the function reaches a value of 1, and becomes undefined as the minimal surface disappears. In the second plot, we see the familiar evidence of collapse, similar to that observed for the Ricci-DeTurck flow for an initial ratio $k^2 = 3$. What this shows is that the addition of the List scalar field *does* affect the long-time existence of the flow, and can lead a geometry whose flow was

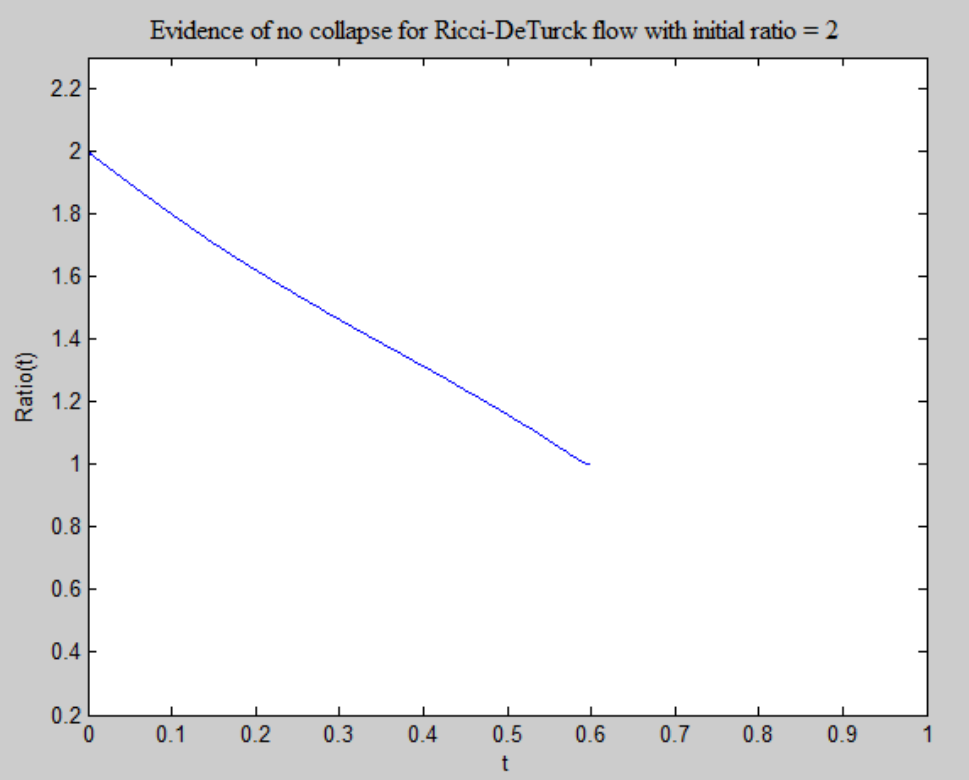

Figure 5.11: *Plotting Ratio(t) for the Ricci-DeTurck flow with* $k^2 = 2$ *shows that this geometry does not collapse.*

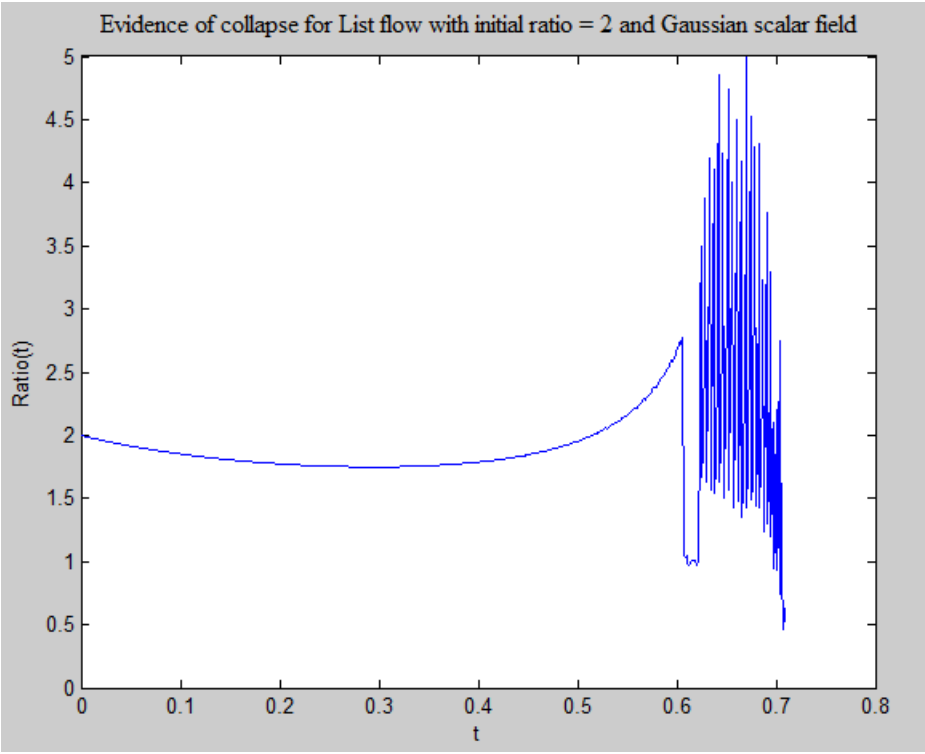

Figure 5.12: *Plotting Ratio(t) for the List flow with* $k^2 = 2$ *and a Gaussian scalar field shows that this geometry does collapse.*

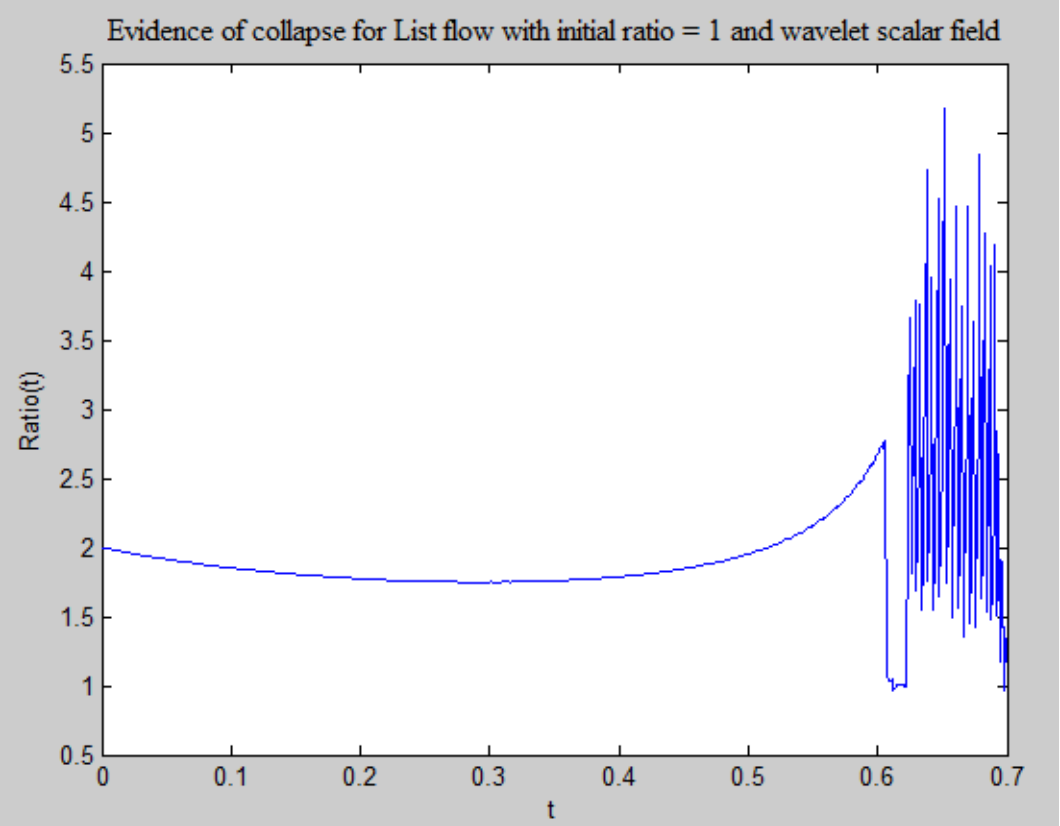

Figure 5.13: *Plotting Ratio(t) for the List flow with $k^2 = 2$ and a wavelet scalar field shows that this geometry also collapses.*

previously immortal to cease fairly quickly due to singularity formation. This behavior does not depend on the scalar field having a specific form, such as being everywhere positive, or Gaussian. Figure 5.13 shows collapse behavior nearly identical to that of the Gaussian case above, but with a wavelet as the initial scalar field (i.e. a Gaussian with the same amplitude and width as we used before, multiplied by $\cos(r)$). In a similar vein, the results obtained in the

case of List flow without a minimal surface do not depend upon a fine-tuning of the scalar field, either in its form or in its specific parameters. Figure 5.14 shows the List flow with $k^2 = 1$, but with a wavelet scalar field similar to that in figure 5.13. As before, the behavior is similar to the case in which $u(t, s)$ is Gaussian.

Finally, we address the question of whether the strong and undesirable assumption of Gulcev, Oliynyk, and Woolgar in [10] was strictly required. That is, does the long-time existence of the rotationally symmetric List flow (in the case of no minimal surface) require the assumption 5.2. We have already shown that the plots of $S(t, s)$ and $A(t, s)$ in such a case suggest long-time existence, but we must also examine the sectional curvatures at the origin to ensure that they do not blow-up in finite time. Moreover, we must do so in a case that violates the above assumption on ∇u. Our simulations suggest that indeed, this assumption is not needed, at least not generally, and figure 5.15 is a representative case. Notice that because of equation 5.3, the geometry in figure 5.15 violates the assumption in [10], and yet appears to exist for all time. This suggests that further analytic progress may be possible in this direction.

5.4 Conclusions

We examined singularity formation in the Ricci-DeTurck flow and the List flow of the bubble, a 1-parameter family of geometries that are intermediate

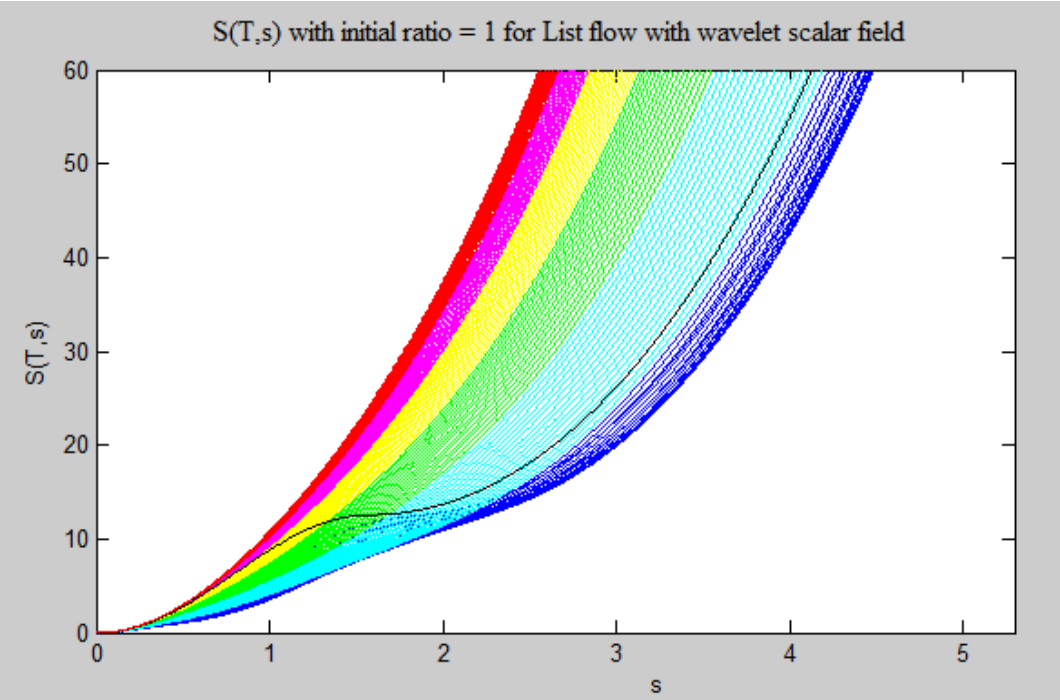

Figure 5.14: *Plotting $S(t, s)$ for the List flow with $k^2 = 1$ and a wavelet scalar field shows that this geometry behaves similarly to the analogous Gaussian case. Recall that the change from blue curves through green, yellow and finally red represents the passage of time from the initial data onward.*

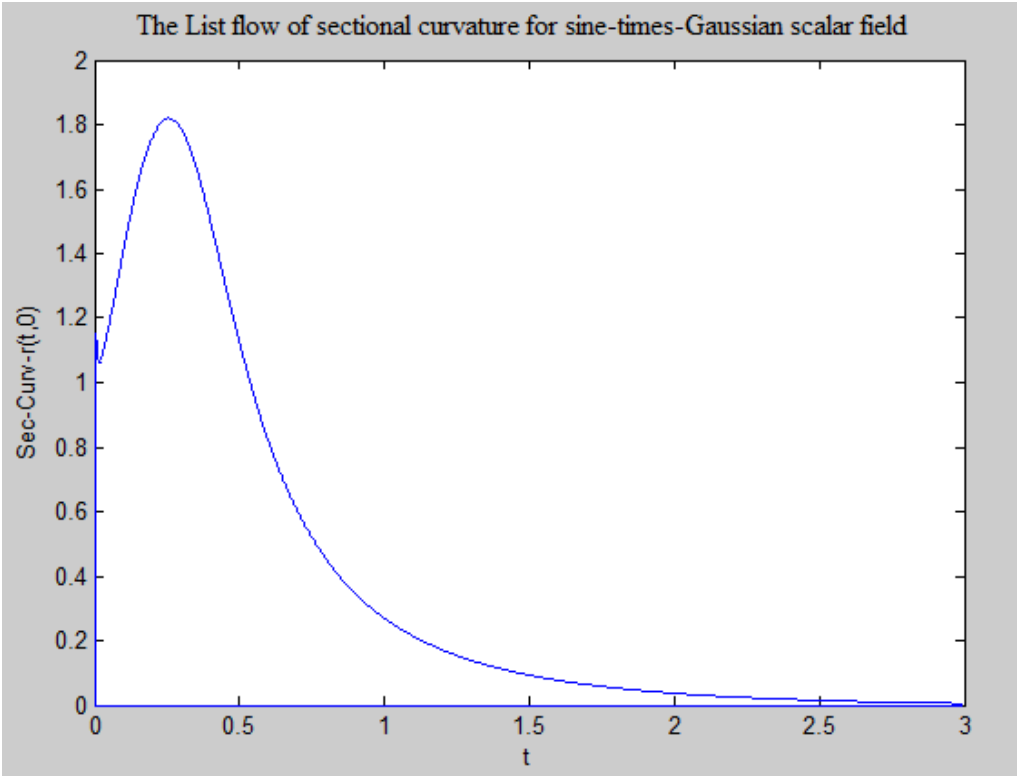

Figure 5.15: *Plotting the sectional curvatures at the origin for the List flow with* $k^2 = 1$ *and a scalar field* $A\sin(r)e^{-(r/\sigma)^2}$ *shows that this geometry behaves similarly to the analogous Gaussian case. The case pictured has* $A = 0.3$ *and* $\sigma = 0.1$*, though similar behavior was observed for all parameter values explored. Note that this geometry does not satisfy the assumption on* ∇u *imposed by Gulcev, Oliynyk, and Woolgar [10], yet their result appears to hold even in this more general case.*

between Garfinkle and Isenberg's corseted spheres, which exhibited threshold behavior, and Balehowsky & Woolgar's Schwarzschild slice, which did not. We found threshold behavior in the case of Ricci-DeTurck flow with a minimal surface, showing smooth long-time evolution for small values of the area ratio k^2, and collapse at the throat for large values. This behavior is similar to that of Garfinkle and Isenberg's corseted spheres, though our manifold was non-compact. In the case of the List flow of the bubble without a minimal surface, we showed that the flow appears to exist for all time, and that it quickly converges to the flat metric on $\mathbb{R}^3$.

We explored the List flow of the bubble with a stable minimal surface, and asked whether the scalar field helped or inhibited collapse. We found that, provided the scalar field was sufficiently large, its effect was to push otherwise stable geometries toward collapse.

Finally, we showed that the analytical results in [10] may hold under more general conditions than those assumed in the authors' proof of the long-time existence of rotationally symmetric List flow. This suggests that additional progress may be made on these questions analytically.

Further numerical explorations could explore possible critical behavior at the threshold point in the case of Ricci-DeTurck flow of the bubble. Does the bubble display critical behavior, similar to that observed in [8], or does collapse immediately change to smooth evolution as we vary k^2? I suspect the

former. Is the critical solution a degenerate neckpinch, modeled on the Bryant soliton, as in [9]? Either answer to any of these questions would be sufficiently interesting to warrant further exploration.

Chapter 6

Appendices

6.1 Appendix A: The Ricci-DeTurck Flow Code

```
function FinalFlow(rPoints,rMax,tPoints,tMax,ratio,graphs)


global rJoin;

global R;

global N;

rJoin = 2*(ratio^(1/3)) -1 -2*(ratio^(1/6))*sqrt((ratio^(1/3))-1)

R = rMax;

N = rPoints;

%r = [linspace(0,R/2,ceil(4*N/5)),...

%linspace(R/2+R/N,R,floor(4*N/5))];
```

```
%Can use this for clustering, if desired
r = linspace(0,R,N);
t = linspace(0,tMax,tPoints);


options = odeset('AbsTol',10^-8, 'RelTol', 10^-8);
sol = pdepe(0,@flowPDE,@pdeic,@pdebc,r,t,options);
A = sol(:,:,1); %size(A) = size(S) = [tPoints, N]
S = sol(:,:,2);


%-------------------------------------------------------------
%Building the arclengths vector
SizeA = size(A);
diexx1 = zeros(1,N);
for i=1:N
    if i<N
        diexx1(i) = r(i+1)-r(i);
    else
        diexx1(i)=diexx1(i-1);
    end
end
diexx = repmat(diexx1,SizeA(1),1);
```

```
expA(:,:) = exp(1).^(A(:,:));

arclengths = zeros(size(A));


arclengths(:,1) = 0;

 for d = 2:N

    arclengths(:,d) = (sum((expA(:,1:d).*diexx(:,1:d))')');

 end

%-------------------------------------------------------------

%The sectional curvatures at r=0


B(:,2) = (1/2)*log(abs(S(:,2)./(4*pi*r(2).*r(2))));


DAT = zeros(tPoints-1);

DBT = zeros(tPoints-1);

for i = 1:tPoints-1

    DAT(i) = (A(i+1,2)-A(i,2))/(tMax/tPoints);

    DBT(i) = (B(i+1,2)-B(i,2))/(tMax/tPoints);

end


SecR = (1/3)*DAT-DBT;

SecTh = (-2/3)*DBT;
```

```
%-------------------------------------------------------------

%Evidence of Collapse


DSR = zeros(tPoints-1,rPoints-1);

for i = 1:rPoints-1

    DSR(:,i) = (S(1:tPoints-1,i+1)-S(1:tPoints-1,i));

end


Pos = DSR>0;

Max = zeros(1,tPoints-1);

Min = zeros(1,tPoints-1);

for j = 1:tPoints-1

    for i = 1:rPoints-2

        if Pos(j,i)==1 && Pos(j,i+1)==0

            Max(j) = S(j,i);

        end

        if Pos(j,i)==0 && Pos(j,i+1)==1

            %i

            Min(j) = S(j,i);

        end

    end
```

```
end

Max = double(Max);

Min = double(Min);

Frac = Max./Min;

%-------------------------------------------------------------

%Plotting the results


for k=1:graphs

    T=ceil(k*tPoints/graphs);


    figure(1)

     if T < ceil(tPoints/6)

    plot(arclengths(T,:),S(T,:));

    elseif T < ceil(2*tPoints/6) && T >= ceil(tPoints/6)

    plot(arclengths(T,:),S(T,:),'c');

    elseif T < ceil(3*tPoints/6) && T >= ceil(2*tPoints/6)

    plot(arclengths(T,:),S(T,:),'g');

    elseif T < ceil(4*tPoints/6) && T >= ceil(3*tPoints/6)

    plot(arclengths(T,:),S(T,:),'y');

    elseif T < ceil(5*tPoints/6) && T >= ceil(4*tPoints/6)

    plot(arclengths(T,:),S(T,:),'m');
```

```
    else
    plot(arclengths(T,:),S(T,:),'r');
    end


    axis([arclengths(1,1), 6.5, 0, 50])
    xlabel('s');
    ylabel('S(T,s)');
    title({'S(T,s) at T=' num2str(k*tMax/graphs)},
    'FontWeight','bold');
    hold on
    grid off
end


for k=1:graphs
    T=ceil(k*tPoints/graphs);


    figure(2)
    if T < ceil(tPoints/6)
    plot(arclengths(T,:),A(T,:));
    elseif T < ceil(2*tPoints/6) && T >= ceil(tPoints/6)
    plot(arclengths(T,:),A(T,:),'c');
```

```
    elseif T < ceil(3*tPoints/6) && T >= ceil(2*tPoints/6)
    plot(arclengths(T,:),A(T,:),'g');
    elseif T < ceil(4*tPoints/6) && T >= ceil(3*tPoints/6)
    plot(arclengths(T,:),A(T,:),'y');
    elseif T < ceil(5*tPoints/6) && T >= ceil(4*tPoints/6)
    plot(arclengths(T,:),A(T,:),'m');
    else
    plot(arclengths(T,:),A(T,:),'r');
    end

    axis([arclengths(1,1), arclengths(1,end), -1.12, 4.5])
    xlabel('s');
    ylabel('A(T,s)');
    title({'A(T,s) at T=' num2str(k*tMax/graphs)},
    'FontWeight','bold');
    hold on
    grid off
end

    figure(3)
    plot(t(1:tPoints-1),Frac);
```

```
    axis([t(1), t(end), 0.2, ratio+0.3])
    title('Evidence of Collapse')
    xlabel('t')
    ylabel('Ratio(t)')
    hold on
    grid off


    figure(4)
    plot(t(1:tPoints-1),SecR,'r')
    plot(t(1:tPoints-1),SecTh)
    axis([0,t(end),-1,8])
    title('Sectional Curvatures at r=0')
    xlabel('t')
    ylabel('Sectional Curvatures(t,0)')
    hold on
    grid off


%-------------------------------------------------------------
function [c f s] = flowPDE(r,t,u,Du)
%Our function is of the form u = [A S]. The PDEs are
%written in the form c*(du/dt) = (d/dr)(f(r,t,u,du/dr))
```

```
%...+s(r,t,u,du/dr)

global R;

global N;

for i=1:length(r)

    if r < 4*R/N

        Bad = 0;

    else

        Bad = (exp(-2*u(1))*(Du(2)^2)/(2*(u(2))^2) +...

              (8*pi/(u(2)))*(-(r/(u(2)))*Du(2)+1));

    end

end

c = [1 1];

f = exp(-2*u(1))*[Du(1) Du(2)];

s = [exp(-2*u(1))*(Du(1)^2)+(8*pi/(u(2)))*(r*Du(1))+Bad,...

    exp(-2*u(1))*(2*Du(1)*Du(2)-(Du(2))^2/(u(2)))+...

    (8*pi*r/(u(2)))*Du(2)-8*pi];

%--------------------------------------------------------

function u0 = pdeic(r)

%This function defines the initial conditions.


global rJoin;
```

```
q = length(r);

A_init=zeros(1,q);

S_init=zeros(1,q);


for i=1:q

   if (abs(r(i))>rJoin)

       S_init(i)=(pi/4)*(r(i))^2*(1+(1/(abs(r(i))))^4;

       A_init(i)=2*log(1+1/(abs(r(i))))-2*log(2);

   else

       S_init(i)=(pi/4)*(r(i))^2*...

       (1+1/rJoin)^6/(1+(r(i))^2/(rJoin^3))^2;

       A_init(i)=3*log(1+1/rJoin)-2*log(2)-...

       log(1+(r(i)^2)/(rJoin^3));

   end

end

u0 = [A_init S_init];

%-------------------------------------------------------------

function [pl ql pr qr] = pdebc(rl,ul,rr,ur,t)

%The boundary conditions are of the form p(r,t,u)+...

%q(r,t)*f(r,t,u,du/dr),

%Left BCs say dA/dr=0 at r=0 & dS(s-->0)=8*pi*s*ds
```

```
pl = [0, -8*pi*rl*exp(ul(1))];

ql = [1, exp(ul(1))];

pr = [8*pi*rr/ur(2)-exp(-ur(1))*sqrt(16*pi/ur(2)),

   -sqrt(16*pi*ur(2))];

qr = [1, exp(ur(1))];
```

6.2 Appendix B: The List Flow Code

```
function FinalFlowList(rPoints,rMax,tPoints,tMax,...

 ratio,graphs,amplitude,width)


global rJoin;

global R;

global N;

global V;

global a;

%For no minimal surface, or non-stable min-surf, use this:

rJoin=2*(ratio^(1/3)) -1 + 2*(ratio^(1/6))*...

sqrt((ratio^(1/3))-1)

%For stable minimal surface, use this:

%rJoin=2*(ratio^(1/3)) -1 - 2*(ratio^(1/6))*...

%sqrt((ratio^(1/3))-1)
```

```
N = rPoints;

R = rMax;

V = amplitude;

a = width;

r = linspace(0,R,N);

t = linspace(0,tMax,tPoints);


options = odeset('AbsTol',10^-8, 'RelTol', 10^-8);

sol = pdepe(0,@flowPDE,@pdeic,@pdebc,r,t,options);

A = sol(:,:,1); %size(A) = size(S) = [tPoints, N]

S = sol(:,:,2);

v = sol(:,:,3);


%-------------------------------------------------------------

%Building the arclengths vector

SizeA = size(A);

diexx1 = zeros(1,N);

for i=1:N

    if i<N

        diexx1(i) = r(i+1)-r(i);

    else
```

```
        diexx1(i)=diexx1(i-1);
    end
end
diexx = repmat(diexx1,SizeA(1),1);
expA(:,:) = exp(1).^(A(:,:));
arclengths = zeros(size(A));


arclengths(:,1) = 0;
 for d = 2:N
    arclengths(:,d) = (sum((expA(:,1:d).*diexx(:,1:d))')');
 end
%-------------------------------------------------------------
%The sectional curvatures at r=0
B(:,2) = (1/2)*log(abs(S(:,2)./(4*pi*r(2).*r(2))));


DAT = zeros(tPoints-2);
DBT = zeros(tPoints-2);
for i = 2:tPoints-1
    DAT(i) = (A(i+1,2)-A(i,2))/(tMax/tPoints);
    DBT(i) = (B(i+1,2)-B(i,2))/(tMax/tPoints);
end
```

```
SecR = (1/3)*DAT-DBT;

SecTh = (-2/3)*DBT;

%-------------------------------------------------------------

%Evidence of Collapse


DSR = zeros(tPoints-1,rPoints-1);

for i = 1:rPoints-1

    DSR(:,i) = (S(1:tPoints-1,i+1)-S(1:tPoints-1,i));

end


Pos = DSR>0;

Max = zeros(1,tPoints-1);

Min = zeros(1,tPoints-1);

for j = 1:tPoints-1

    for i = 1:rPoints-2

        if Pos(j,i)==1 && Pos(j,i+1)==0

            Max(j) = S(j,i);

        end

        if Pos(j,i)==0 && Pos(j,i+1)==1

            %i
```

```
            Min(j) = S(j,i);
        end
    end
end
Max = double(Max);
Min = double(Min);
Frac = Max./Min;
%-------------------------------------------------------------
%Plotting the results

for k=1:graphs
    T=ceil(k*tPoints/graphs);

    figure(1)
    %plot(arclengths(1,:),4*pi*arclengths(1,:).^2,'k');
    plot(arclengths(1,:),S(1,:),'k');
    if T < ceil(tPoints/6)
    plot(arclengths(T,:),S(T,:));
    elseif T < ceil(2*tPoints/6) && T >= ceil(tPoints/6)
    plot(arclengths(T,:),S(T,:),'c');
    elseif T < ceil(3*tPoints/6) && T >= ceil(2*tPoints/6)
```

```
    plot(arclengths(T,:),S(T,:),'g');
    elseif T < ceil(4*tPoints/6) && T >= ceil(3*tPoints/6)
    plot(arclengths(T,:),S(T,:),'y');
    elseif T < ceil(5*tPoints/6) && T >= ceil(4*tPoints/6)
    plot(arclengths(T,:),S(T,:),'m');
    else
    plot(arclengths(T,:),S(T,:),'r');
    end

    axis([arclengths(1,1), 6.5, 0, 60])
    xlabel('s');
    ylabel('S(T,s)');
    title({'S(T,s) at T=' num2str(k*tMax/graphs)},
    'FontWeight','bold');
    hold on
    grid off
end

for k=1:graphs
    T=ceil(k*tPoints/graphs);
```

```
figure(2)

plot(arclengths(1,:),A(1,:),'k');

if T < ceil(tPoints/6)

plot(arclengths(T,:),A(T,:));

elseif T < ceil(2*tPoints/6) && T >= ceil(tPoints/6)

plot(arclengths(T,:),A(T,:),'c');

elseif T < ceil(3*tPoints/6) && T >= ceil(2*tPoints/6)

plot(arclengths(T,:),A(T,:),'g');

elseif T < ceil(4*tPoints/6) && T >= ceil(3*tPoints/6)

plot(arclengths(T,:),A(T,:),'y');

elseif T < ceil(5*tPoints/6) && T >= ceil(4*tPoints/6)

plot(arclengths(T,:),A(T,:),'m');

else

plot(arclengths(T,:),A(T,:),'r');

end


axis([arclengths(1,1), arclengths(1,end), -1.12, 4.5])

xlabel('s');

ylabel('A(T,s)');

title({'A(T,s) at T=' num2str(k*tMax/graphs)},

'FontWeight','bold');
```

```
    hold on
    grid off
end


for k=1:graphs
    T=ceil(k*tPoints/graphs);


    figure(3)
    plot(arclengths(1,:),v(1,:),'k');
    if T < ceil(tPoints/6)
    plot(arclengths(T,:),v(T,:));
    elseif T < ceil(2*tPoints/6) && T >= ceil(tPoints/6)
    plot(arclengths(T,:),v(T,:),'c');
    elseif T < ceil(3*tPoints/6) && T >= ceil(2*tPoints/6)
    plot(arclengths(T,:),v(T,:),'g');
    elseif T < ceil(4*tPoints/6) && T >= ceil(3*tPoints/6)
    plot(arclengths(T,:),v(T,:),'y');
    elseif T < ceil(5*tPoints/6) && T >= ceil(4*tPoints/6)
    plot(arclengths(T,:),v(T,:),'m');
    else
    plot(arclengths(T,:),v(T,:),'r');
```

```
    end


    axis([arclengths(1,1), arclengths(1,N)-0.25,
    -0.01, amplitude])
    xlabel('s');
    ylabel('v(T,s)');
    title({'v(T,s) at T=' num2str(k*tMax/graphs)},
    'FontWeight','bold');
    hold on
    grid off
end


    figure(4)
    plot(t(1:tPoints-1),Frac);
    title('Evidence of Collapse')
    xlabel('t')
    ylabel('Ratio(t)')
    hold on
    grid off


    figure(5)
```

```
    plot(t(2:tPoints-1),SecR)
    %axis([0,t(end),-0.5,2.5])
    title('Sec-Curv-r at r=0')
    xlabel('t')
    ylabel('Sec-Curv-r(t,0)')
    hold on
    grid off


%-------------------------------------------------------------
function [c f s] = flowPDE(r,t,u,Du)
%Our function is of the form u = [A S]. The PDEs are
%written in the form c*(du/dt) = (d/dr)(f(r,t,u,du/dr))+...
s(r,t,u,du/dr)
global R;
global N;
for i=1:length(r)
    if r(i) < 4*R/N
        Bad = 0;
    else
        Bad = (exp(-2*u(1))*(Du(2)^2)/(2*(u(2))^2)+...
         (8*pi/(u(2)))*(-(r/(u(2)))*Du(2)+1));
```

```
    end
end
c = [1 1 1];
f = exp(-2*u(1))*[Du(1) Du(2) Du(3)];
s = [exp(-2*u(1))*(Du(1)^2 + 2*(Du(3))^2)+...
(8*pi/(u(2)))*(r*Du(1))+Bad, ...
    exp(-2*u(1))*(2*Du(1)*Du(2)-(Du(2))^2/(u(2)))+...
    (8*pi*r/(u(2)))*Du(2)-8*pi,...
    exp(-2*u(1))*(2*Du(1)-(Du(2))/u(2))+8*pi*r/u(2)];
%-------------------------------------------------------------
function u0 = pdeic(r)
%This function defines the initial conditions.


global rJoin;
global V;
global a;
q = length(r);
A_init=zeros(1,q);
S_init=zeros(1,q);
v_init=zeros(1,q);
```

```
for i=1:q

    %Gaussian

    %v_init=V*exp(-(r(i)/a)^2);

    %Wavelet

    v_init=V*exp(-(r(i)/a)^2)*sin(r(i));

   if (abs(r(i))>rJoin)

       S_init(i)=(pi/4)*(r(i))^2*...

       (1+(1/(abs(r(i)))))^4;

       A_init(i)=2*log(1+1/(abs(r(i))))-2*log(2);

   else

       S_init(i)=(pi/4)*(r(i))^2*(1+...

       1/rJoin)^6/(1+(r(i))^2/(rJoin^3))^2;

       A_init(i)=3*log(1+1/rJoin)-2*log(2)-...

       log(1+(r(i))^2/(rJoin^3));

   end


end


u0 = [A_init S_init v_init];

%-------------------------------------------------------------

function [pl ql pr qr] = pdebc(rl,ul,rr,ur,t)
```

```
%The boundary conditions are of the form p(r,t,u)+...

%q(r,t)*f(r,t,u,du/dr),

pl = [0, -8*pi*rl*exp(ul(1)), 0];

ql = [1 exp(ul(1)) 1];

pr = [8*pi*rr/ur(2)-exp(-ur(1))*sqrt(16*pi/ur(2)),

-sqrt(16*pi*ur(2)), ur(3)];

qr = [1, exp(ur(1)), 0];
```

Bibliography

[1] MM Akbar and E Woolgar, *Ricci Solitons and Einstein-Scalar Field Theory*, Class Quantum Gravit 26 (2009) 055015 [arxiv:0808.3126].

[2] T Balehowsky and E Woolgar. *The Ricci flow of the $\mathbb{RP}^3$-geon and non-compact manifolds with essential minimal spheres.* arXiv:1004.1833v1 [math.DG]

[3] Bennett Chow and Dan Knopf. *The Ricci flow: an introduction*, volume 110 of Mathematical Surveys and Monographs. American Mathematical Society, Providence, RI, 2004.

[4] Bennett Chow, Peng Lu, and Lei Ni. *Hamilton's Ricci Flow.* Science Press, Beijing, 2006.

[5] DeTurck, Dennis M. *Deforming metrics in the direction of their Ricci tensors.* J Differential Geom. **18** (1983), no. 1, 157–162.

[6] P Figueras, J Lucietti, T Wiseman *Ricci solitons, Ricci flow, and strongly coupled CFT in the Schwarzschild Unruh or Boulware vacua*, arXiv:1104.4489v1 [hep-th] 22 Apr (2011).

[7] DH Friedan, PhD thesis, Berkeley (1980), unpublished; Phys Rev Lett 45 (1980) 1057; Ann Phys (NY) 163 (1985) 318.

[8] D Garfinkle and J Isenberg, *Critical behavior in Ricci flow*, in Geometric Evolution Equations, Contemp Math 367 (2005) 103–114, eds S-C Chang, B Chow, S-C Chu, C-S Lin (AMS, Providence) [arxiv.org:math/0306129].

[9] D Garfinkle and J Isenberg, *The Modelling of Degenerate Neck Pinch Singularities in Ricci Flow by Bryant Solitons*, Journal of Mathematical Physics 49 (2008) 073505 [arXiv:0709.0514].

[10] L Gulcev, TA Oliynyk, and E Woolgar, *On long-time existence for the flow of static metrics with rotational symmetry*, Commun Anal Geom, 18 (2010) 705 [arxiv:0911.2037].

[11] Hamilton, Richard S. *Three-manifolds with positive Ricci curvature.* J Differential Geom. **17** (1982), no. 2, 255–306.

[12] B List, *Evolution of an extended Ricci flow system*, Commun Anal Geom 16 (2008) 1007–1048.

[13] John Morgan and Gang Tian. *Ricci Flow and the Poincare Conjecture*. American Mathematical Society, Providence, RI, 2007.

[14] MathWorks^{TM}, *R2011b Documentation − MATLAB − pdepe*, `http://www.mathworks.com/help/techdoc/ref/pdepe.html`, Retrieved August 5 (2011).

[15] G Perelman, *The Entropy Formula for the Ricci Flow and its Geometric Applications*. arXiv:math/0211159v1 [math.DG] 11 Nov (2002).

[16] G Perelman, *Ricci flow with surgery on three-manifolds*. arXiv:math/0303109v1 [math.DG] 10 Mar (2003).

[17] G Perelman, *Finite extinction time for the solutions to the Ricci flow on certain three-manifolds*. arXiv:math/0307245v1 [math.DG] 17 Jul (2003).

[18] TA Oliynyk and E Woolgar, *Rotationally symmetric Ricci flow on asymptotically flat manifolds*, Commun Anal Geom 15 (2007) 535–568 [arxiv:math/0607438].

[19] J.H. Rubinstein and R. Sinclair; *Visualizing Ricci Flow of Manifolds of Revolution*, Experimental Mathematics, Vol. 14, No. 3 (2005) 285–298 [arXiv:math.DG/0406189v1].

[20] T Wiseman, *Numerical construction of static and stationary black holes*, Chapter in *Black Holes in Higher Dimensions* to be published by Cambridge University Press (editor: G. Horowitz)
Preprint: arXiv:1107.5513v1 [gr-qc] 27 Jul (2011).

[21] E Woolgar, *Some Applications of Ricci Flow in Physics*, Proc Theory Canada III workshop, Can J Phys 86 (2008) 645 [arxiv:0708.2144].